Plasma-Dust Coupling in the Heliosphere

Christoph Lhotka,
University of Rome Tor Vergata

The heliospheric space plasma physics in the era of multipoint space missions

Palazzo Camponeschi, L'Aquila 2026

Topics of interest…

Dust in space

- Where can it be found ?
- Natural sources
- Human made dust
- Danger of space dust

Space weather

- Effect on dust dynamics
- Solar wind models
- Interplanetary magnetic field

Force models

- Non gravitational forces
- Gauss' equations
- Near Hamiltonian framework

Solar radiation

- Poynting-Robertson effect
- Solar radiation pressure
- Solar wind drag

Charged dust grains

- Charging processes
- Secular evolution
- Distribution, bands

Role of resonances

- Mean motion resonances
- Temporary capture
- Stability

Dust in the solar system

Dust rings are found in the solar system and also in exo-planetary systems.

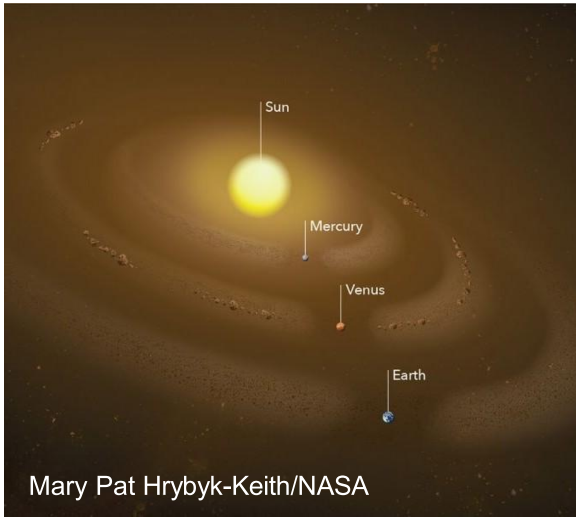

Stenborg et al. 2018, Pokorny & Kuchner 2019

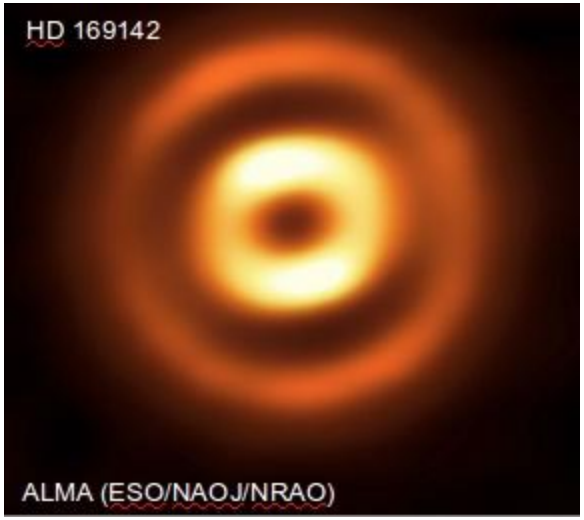

Fedele et al. 2017

several µm

... nanometers → 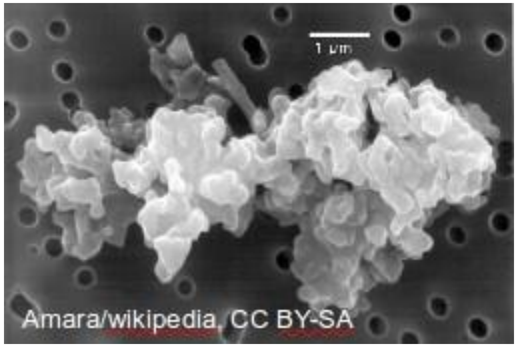 → millimetres ...

Debris and dust sources

Debris and dust is constantly produced and removed from space

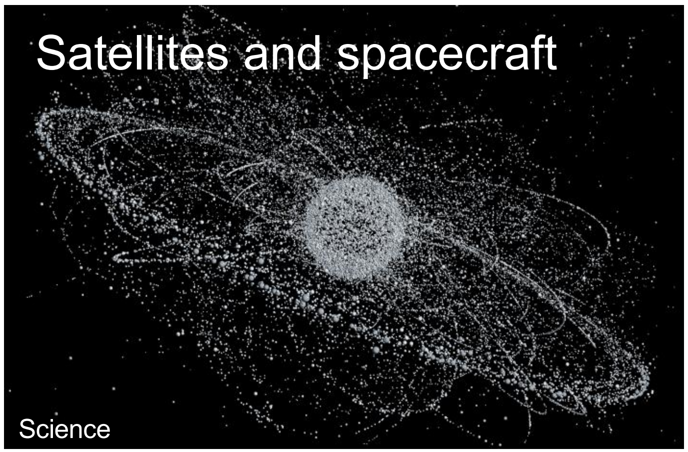

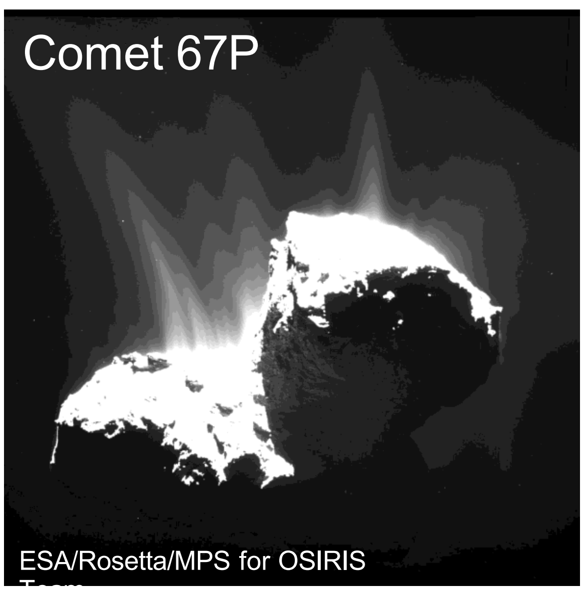

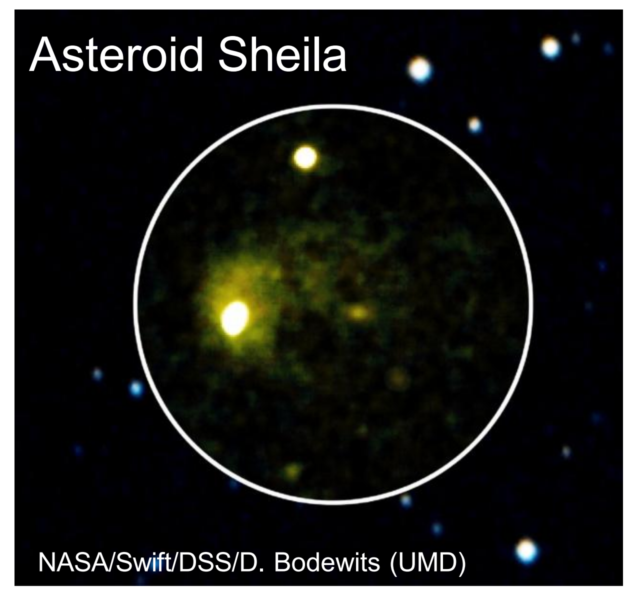

Space debris and space dust

Al2O3 particles

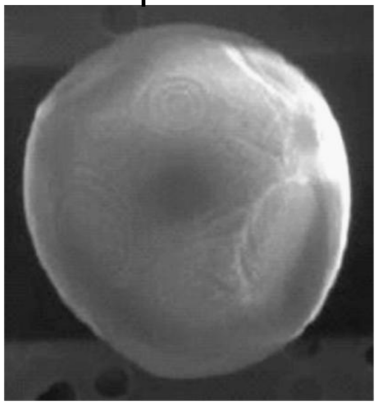

Micrometeorites

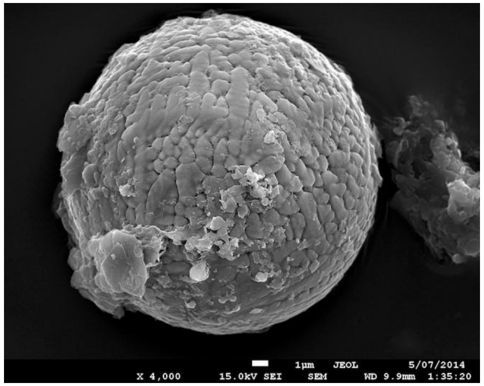

Paint flake

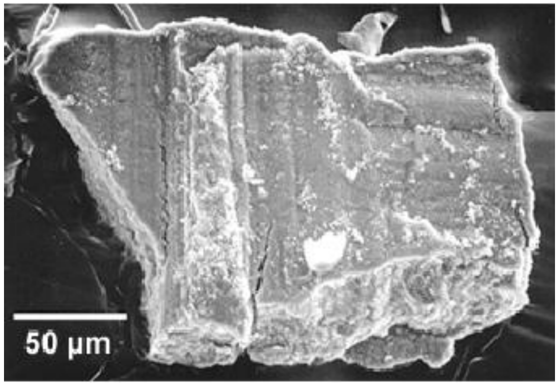

Asteroidal dust

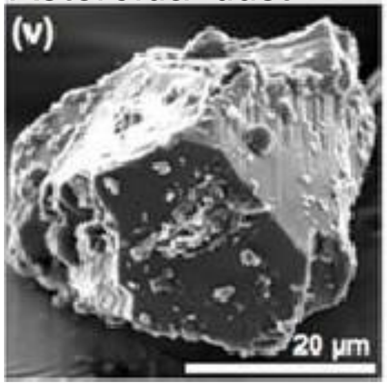

Exhaust slag

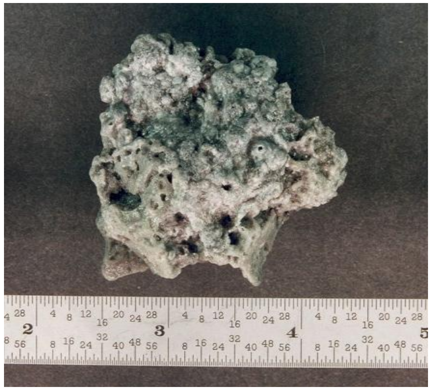

Cometary dust

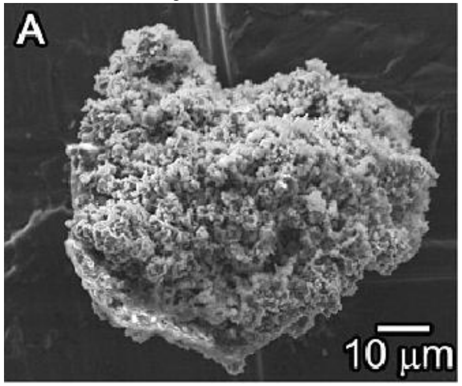

1) Al_2O_3 particles from rocket science lab vs. micrometeorite in 2.7 billion old lime stone in Western Australia

2) Paint flake from impactor analysis of Space Shuttle vs. asteroidal dust from 25143 Itokawa, Hayabusa probe

3) Exhaust slag from NASA vs. comet dust in antarctic ice near Tottuki Point

Serious damage to spacecraft

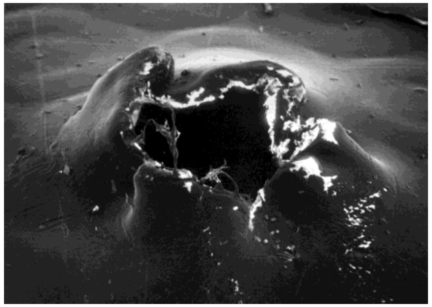

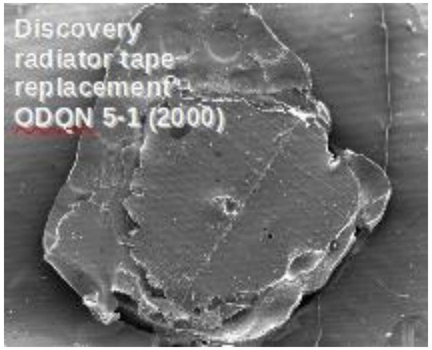

Hypervelocity impacts on space shuttle (STS-87) :

Probably due to 0.1mm stainless steel impactor

7 impacts with 1mm minimum radius on radiators (176 impacts on windows)

Damage regions from 0.125 to 3.25mm

Orbital debris 24 vs. meteoroids 28 (out of 52)

71% aluminum, 21% stainless steel, 8% paint flakes

ODQN 3-4 (1998).

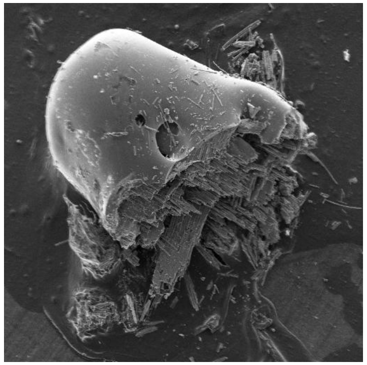

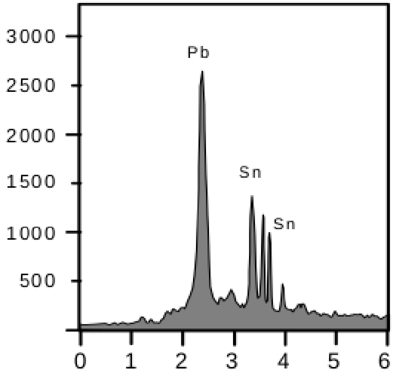

James Webb space telescope

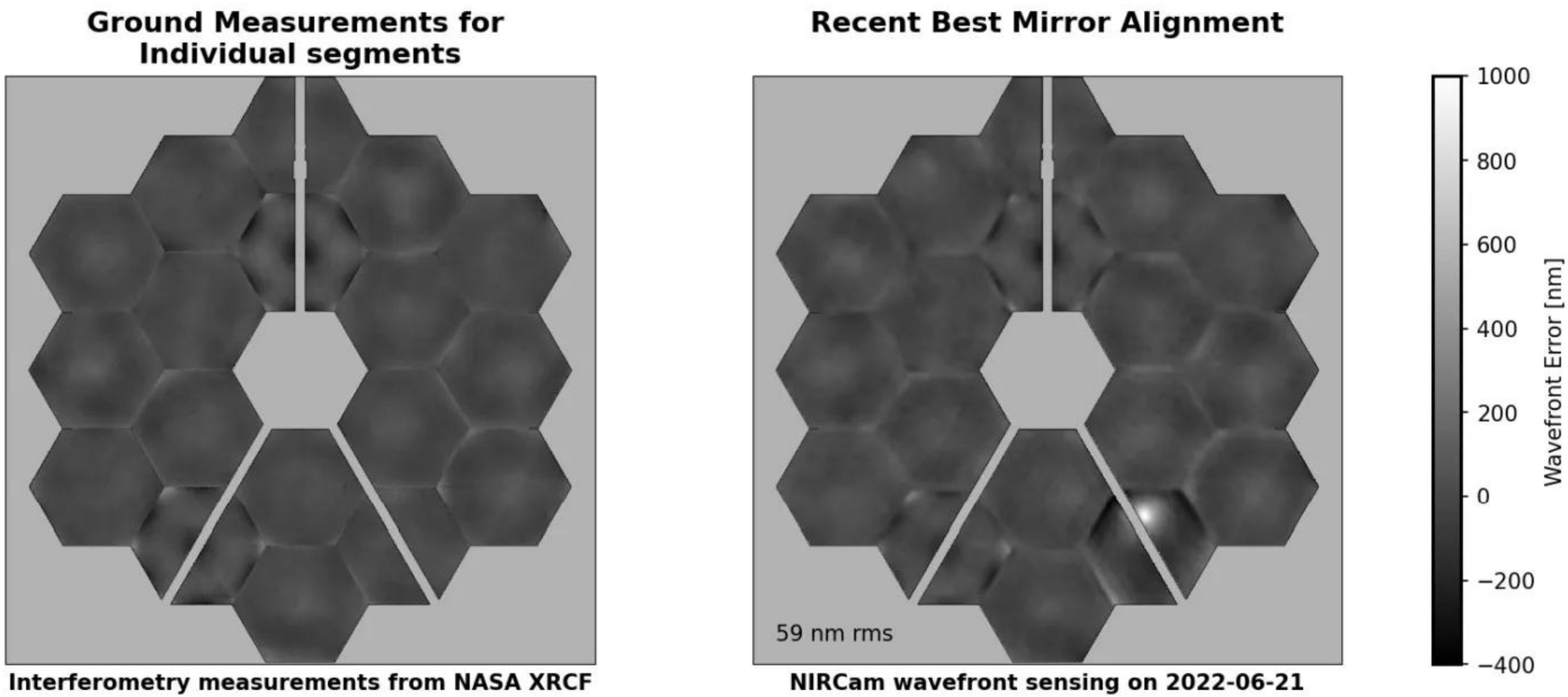

On the right, the state of the James Webb Space Telescope on June 21, 2022, after an unexpectedly large micrometeoroid strike and subsequent responses, compared to the expected state on the left. (Image credit: NASA/STScI)

Affects space measurements

$$1 - \alpha_0 e^{-z_0} - \beta_0 e^{\frac{V_0}{V_1} z_0} + \alpha_1 z_0 = 0$$

Reconstruction of spacecraft potential

$$t_c \propto \frac{1}{\alpha_p \left(\alpha_0 e^{-z_0} + \alpha_1 + \beta_0 \frac{V_0}{V_1} e^{-\frac{V_0}{V_1} z_0} \right)}$$

Charging time scale
- time series

Lhotka et al. 2020

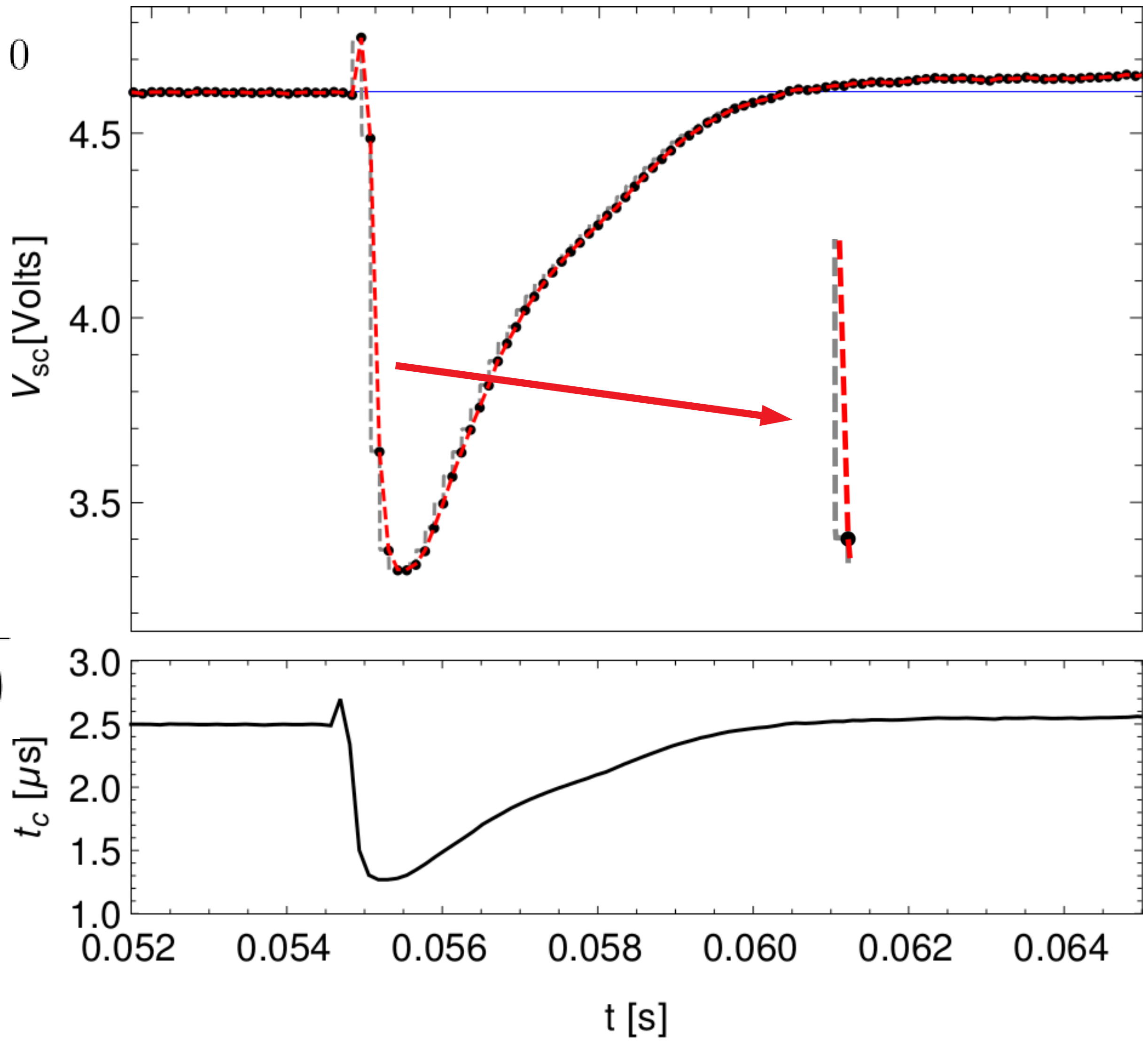

Forces, orbital motion

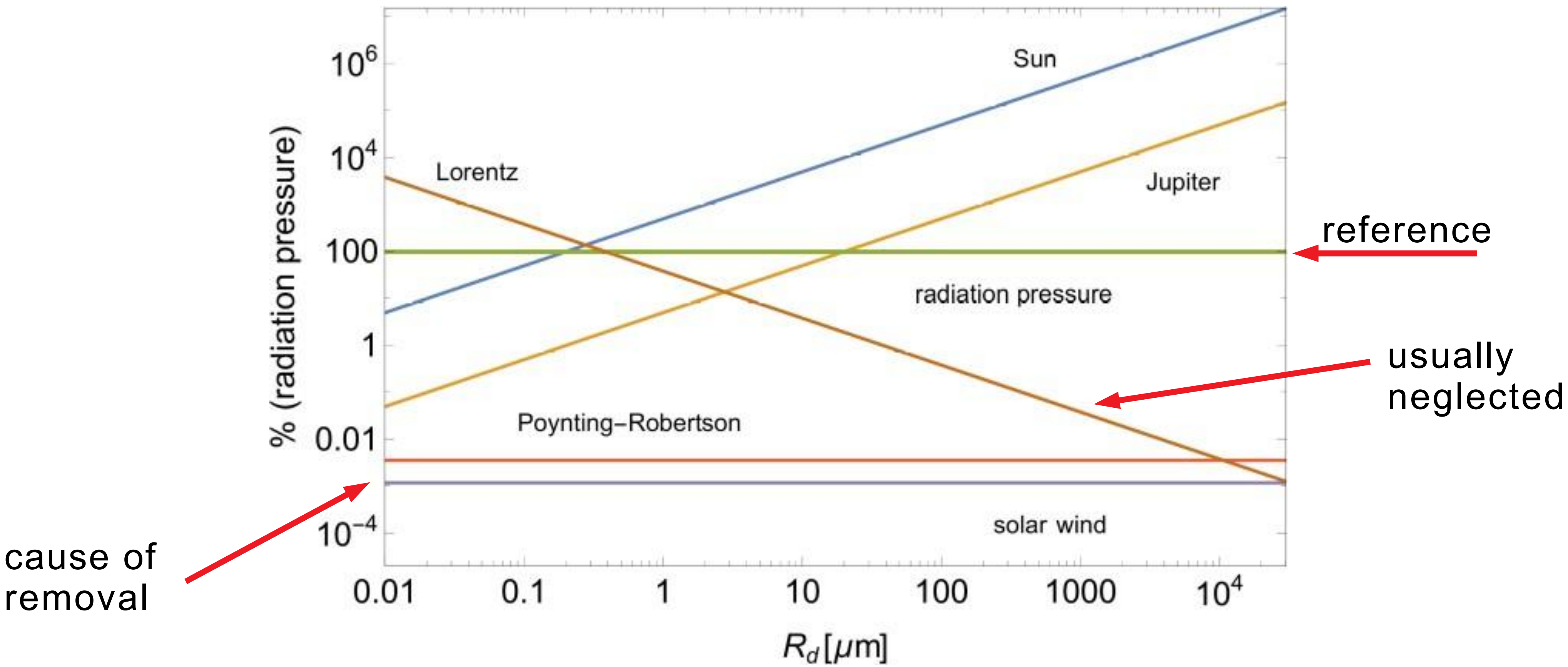

Force magnitudes evaluated for dust grains with 2.8 gcm^{-3} density at a distance of 8AU from the sun (depends on distance etc..)

Lorentz force, really ?

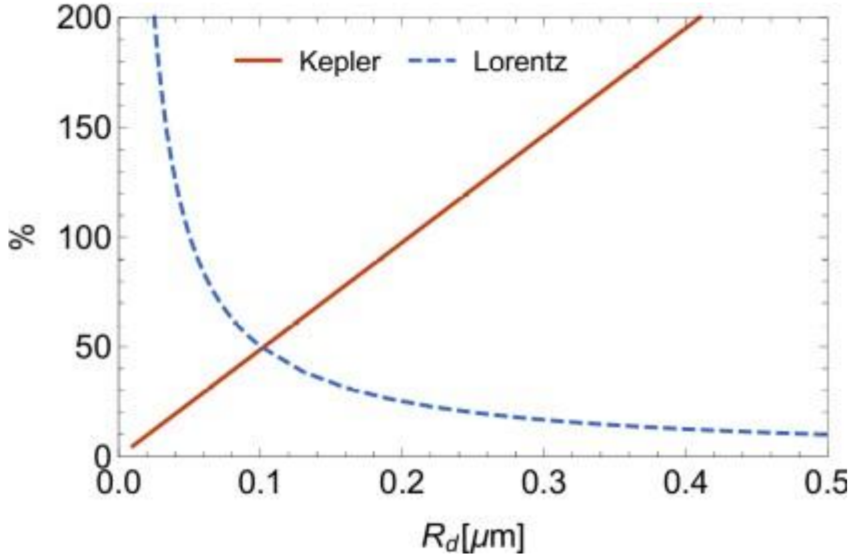

- Lorentz force is stronger in magnitude than central gravity for tiny particles
- Solar radiation pressure is dominant still for smaller particles
- Effect of Jupiter (evaluated at Earth orbit) is weaker for micro-meter sized particles than LF
- Lorentz force is the dominant non-gravitational force up to 400 micro-meters (without SRP)

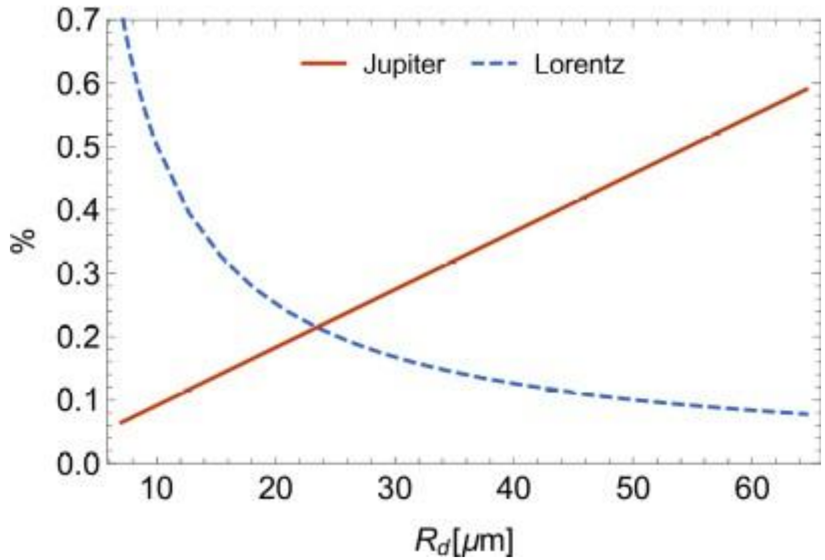

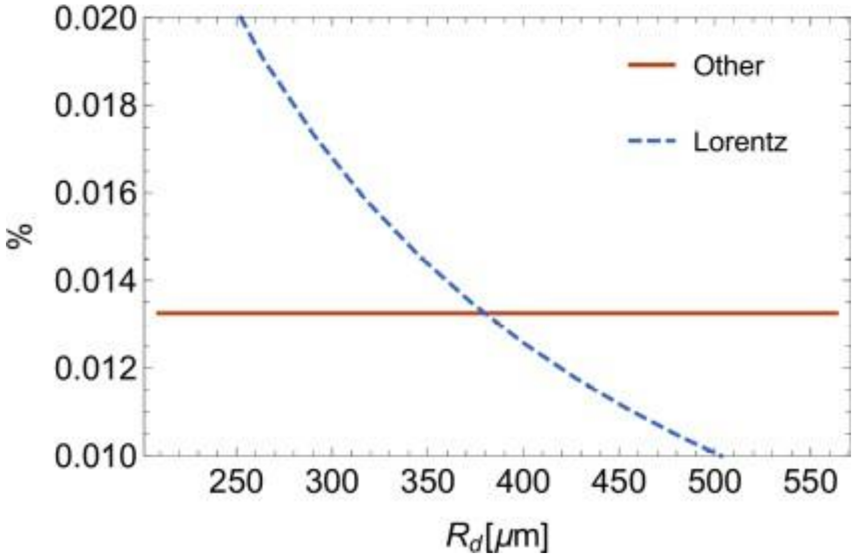

Dynamics in the solar system

Charged particle subject to planet, solar wind, and interplanetary magnetic field:

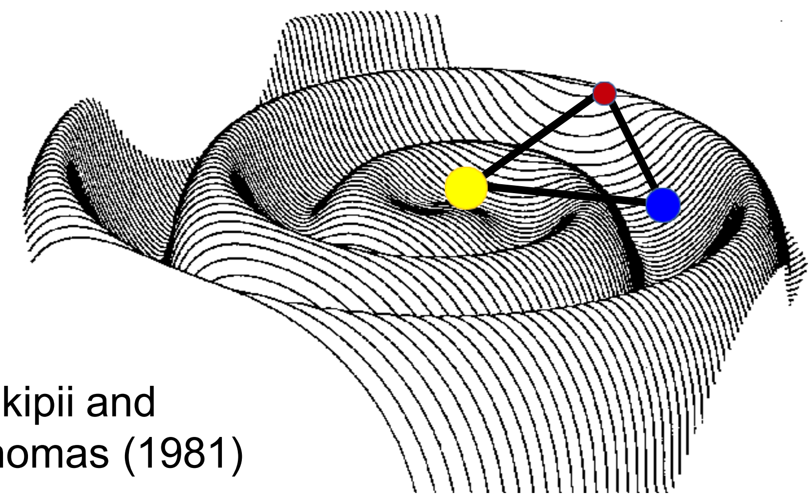

Jokipii and Thomas (1981)

$$\frac{d\mathbf{v}}{dt} = \overset{(1)}{-\frac{(1-\beta)\mu}{r^2}\mathbf{e}_R} - \overset{(2)}{\frac{\beta\mu}{r^2}\left(1+\frac{\eta}{Q}\right)\left(\frac{(\mathbf{v}\cdot\mathbf{e}_R)\mathbf{e}_R+\mathbf{v}}{c}\right)}$$

$$- \overset{(3)}{Gm_1\left(\frac{\mathbf{r}_1}{r_1^3}+\frac{\mathbf{r}-\mathbf{r}_1}{\|\mathbf{r}-\mathbf{r}_1\|^3}\right)} + \overset{(4)}{\frac{q}{m}(\mathbf{v}-\mathbf{u}_{sw})\times\mathbf{B}},$$

Gravitational attraction of the sun (1), Poynting-Robertson and solar wind drag (2), the attraction of an additional planet (3), and Lorentz force due to the interplanetary magnetic field (4)

- Effect of (1) : two body motion with reduced central mass.
- Effect of (2) : e.g, inward drift in semi-major axis due to loss of orbital energy.
- Effect of (3) : e.g., temporary capture in orbital resonance with the planets.
- Effect of (4) : e.g., inward/outward drift in semi-major axis / off plane motion.

Dynamics around planets

Poynting-Robertson and solar wind drag in the space debris problem :

$$\ddot{x} = V_x(x, y, z, \theta)^{(1)} - \mathcal{G} m_S \left(\frac{x - x_S}{|\boldsymbol{r} - \boldsymbol{r}_S|^3} + \frac{x_S}{r_S^3} \right)^{(2)} - \mathcal{G} m_M \left(\frac{x - x_M}{|\boldsymbol{r} - \boldsymbol{r}_M|^3} + \frac{x_M}{r_M^3} \right)^{(3)} + \beta \mathcal{G} m_S \frac{x - x_S}{|\boldsymbol{r} - \boldsymbol{r}_S|^3}^{(4)} - \frac{\beta \mathcal{G} m_S}{c}^{(5)} \left(1 + \frac{\eta}{Q} \right)^{(6)} \left\{ \frac{x - x_S}{|\boldsymbol{r} - \boldsymbol{r}_S|^3} (\dot{x} - \dot{x}_S) + \frac{\dot{x} - \dot{x}_S}{|\boldsymbol{r} - \boldsymbol{r}_S|^2} \right\}$$

Force (per unit mass) due to *gravitational potential of the Earth* (1), *Sun's gravity* (2), the *attraction of the Moon* (3), *solar radiation pressure* (4), *Poynting-Robertson drag* (5), and *solar wind drag* (6).

Effect of (5) + (6) :

- Leads to drift in semi-major axis a
- Shifts the location of resonant equilibria, i.e. the location of geostationary orbit
- May render stationary orbits unstable and leads to temporary capture

Lhotka, Celletti, Gales, MNRAS 460, 802–815 (2016)

Gauss' planetary equations of motions

Perturbation theory in Gauss form of equations of motion :

$$\ddot{\boldsymbol{r}} = -\frac{\mu}{r^2}\boldsymbol{e}_R + \boldsymbol{F}(\boldsymbol{r}, \dot{\boldsymbol{r}}, r, \dot{r}, \cos\psi, \ldots)$$

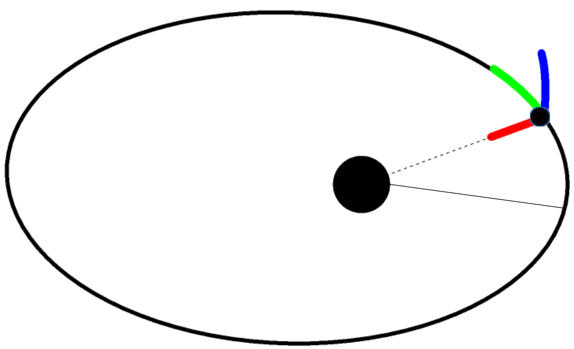

radial $\boldsymbol{o}_{\mathrm{R}} = (\cos f, \sin f, 0)$

tangential $\boldsymbol{o}_{\mathrm{T}} = (-\sin f, \cos f, 0)$

normal $\boldsymbol{e}_{\mathrm{N}} = \boldsymbol{o}_{\mathrm{R}} \times \boldsymbol{o}_{\mathrm{T}}$

force system

$$\mathfrak{F} = \mathfrak{F}_{\mathrm{R}}\boldsymbol{o}_{\mathrm{R}} + \mathfrak{F}_{\mathrm{T}}\boldsymbol{o}_{\mathrm{T}} + \mathfrak{F}_{\mathrm{N}}\boldsymbol{o}_{\mathrm{N}}$$

$$\frac{\mathrm{d}a}{\mathrm{d}t} = \frac{2ah}{\mu\left(1-e^2\right)}\left[e\sin f\,\mathfrak{F}_{\mathrm{R}} + (1+e\cos f)\,\mathfrak{F}_{\mathrm{T}}\right],$$

$$\frac{\mathrm{d}e}{\mathrm{d}t} = \frac{h}{\mu}\left[\sin f\,\mathfrak{F}_{\mathrm{R}} + (\cos f + \cos E)\,\mathfrak{F}_{\mathrm{T}}\right],$$

$$\frac{\mathrm{d}i}{\mathrm{d}t} = \frac{\cos(\omega+f)\,r}{h}\mathfrak{F}_{\mathrm{N}},$$

$$\frac{\mathrm{d}\omega}{\mathrm{d}t} = -\frac{h}{\mu}\frac{1}{e}\left[\cos f\,\mathfrak{F}_{\mathrm{R}} - \left(\frac{2+e\cos f}{1+e\cos f}\right)\sin f\,\mathfrak{F}_{\mathrm{T}}\right] - \frac{\cos i\,\sin(\omega+f)\,r\,\mathfrak{F}_{\mathrm{N}}}{h\sin i},$$

$$\frac{\mathrm{d}\Omega}{\mathrm{d}t} = \frac{\sin(\omega+f)\,r}{h\sin i}\mathfrak{F}_{\mathrm{N}},$$

$$\frac{\mathrm{d}M}{\mathrm{d}t} = n + \frac{h}{\mu}\frac{\sqrt{1-e^2}}{e}\left[\left(\cos f - \frac{2e}{1-e^2}\frac{r}{a}\right)\mathfrak{F}_{\mathrm{R}} - \left(1 + \frac{1}{1-e^2}\frac{r}{a}\right)\sin f\,\mathfrak{F}_{\mathrm{T}}\right].$$

Local force system attached to celestial body

Near Hamiltonian system

Many applications in celestial mechanics can be described by nearly integrable, weakly dissipative systems :

Hamiltonian dynamics:

$$H(y,x,t) = H_0(y) + \varepsilon H_1(y,x,t)$$

analytic, regular functions H_0, H_1

$y \in \mathbb{R}^\ell$, $(x,t) \in \mathbb{T}^{\ell+1}$ action-angle like variables

fundamental frequencies:

$$\omega(y) = \partial H_0(y)/\partial y$$

for $\varepsilon = 0$ integrable:

$$\begin{aligned} x(t) &= x(0) + \omega(y(0))t \\ y(t) &= y(0)\ , \end{aligned}$$

Nearly Hamiltonian = weakly dissipative:

$$H(y,x,t) = h_{00}(y) + \varepsilon h_{10}(y,x,t)$$

$$\begin{aligned} \dot{x} &= \omega(y) + \varepsilon h_{10,y}(y,x,t) + \mu f_{01}(y,x,t) \\ \dot{y} &= -\varepsilon h_{10,x}(y,x,t) + \mu\Big(g_{01}(y,x,t) - \eta(y,x,t)\Big) \end{aligned}$$

$\rightarrow$ for $\varepsilon = 0$ dissipative, possibly integrable

$\rightarrow$ for $\mu = 0$ conservative

$\rightarrow$ for $\varepsilon = \mu = 0$ integrable

drift function:

$$\eta = \eta(y,x,t)$$

analytic, regular functions h_{10}, f_{01}, g_{01}

Tools from Hamiltonian dynamics are useful also for dissipative systems (and vice versa).

Celletti, A., Lhotka, C., 2013, Lhotka, C., Celletti, A., 2014

Gravity

mass of dust

gravitational parameter

mass of secondary

$$\mathbf{F}_g = -\frac{\mu m}{r^3}\mathbf{r} - \frac{\mu m_1 m}{m_0}\left(\frac{\mathbf{r}_1}{r_1^3} + \frac{\mathbf{r}-\mathbf{r}_1}{\|\mathbf{r}-\mathbf{r}_1\|^3}\right)$$

mass of primary

secondary's distance

distance of dust from primary

Basic model: spatial restricted three-body problem

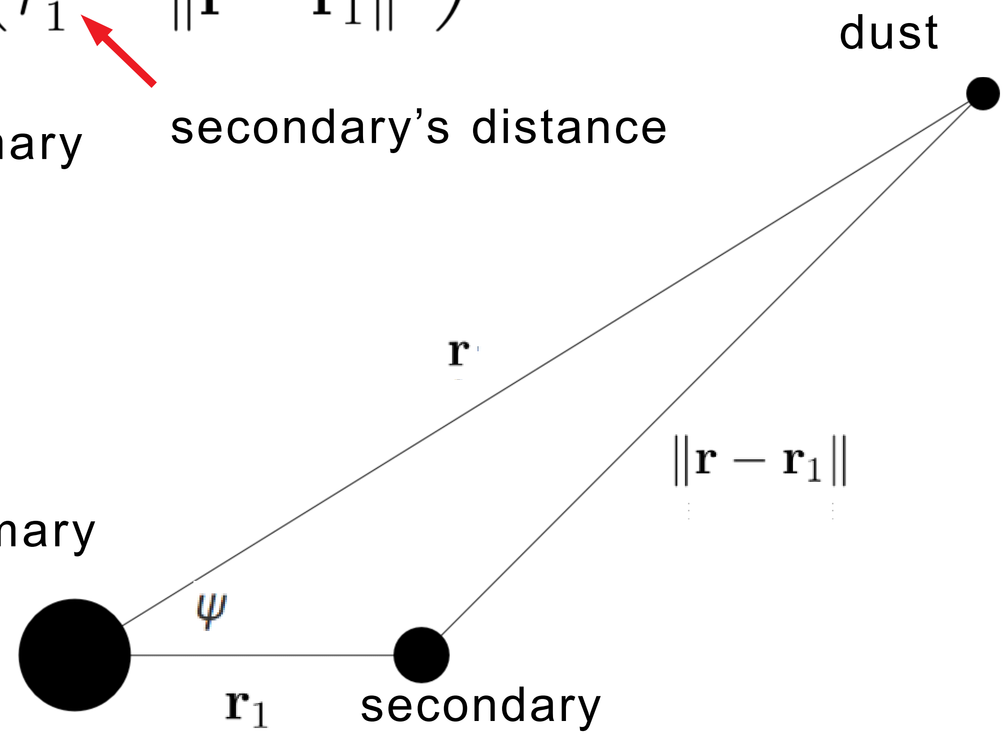

In solar system dynamics:
- primary : sun
- secondary : Jupiter

Extra-planetary systems:
- primary : star
- secondary : main planet

Solar radiation

<u>solar radiation</u>
solar gravity

mass of dust

solar wind factor

velocity vector

$$\mathbf{F}_{s/p} = -\nabla \frac{\mu m \beta}{r} - \frac{\mu m \beta}{r^2}\left(1+\frac{\eta}{Q}\right)\left(\frac{(\dot{\mathbf{r}}\cdot\mathbf{g}_r)\,\mathbf{g}_r + \dot{\mathbf{r}}}{c}\right)$$

gravitational parameter

efficiency factor

speed of light

radial unit vector

distance of dust from primary

relativistic derivation:

$$\frac{dp^{\mu}_{in}}{d\tau} = \frac{w^2 S A' \overline{Q}'_{ext}}{c} b^{\mu}$$

τ proper time

$$\frac{dp^{\mu}_{out}}{d\tau} = \frac{w^2 S A' \overline{Q}'_{ext}}{c}\left[\overline{Q}'\frac{u^{\mu}}{c} + \left(1-\overline{Q}'\right)b^{\mu}\right]$$

$$\frac{dp^{\mu}}{d\tau} = \frac{dp^{\mu}_{in}}{d\tau} - \frac{dp^{\mu}_{out}}{d\tau}$$

equation of motion

Newtonian approximation:

$$\boxed{\frac{d\vec{v}}{dt} = \frac{S A' \overline{Q}'_{pr}}{mc}\left[\left(1-\frac{\vec{v}\cdot\vec{e}}{c}\right)\vec{e} - \frac{\vec{v}}{c}\right]}$$

incident photons

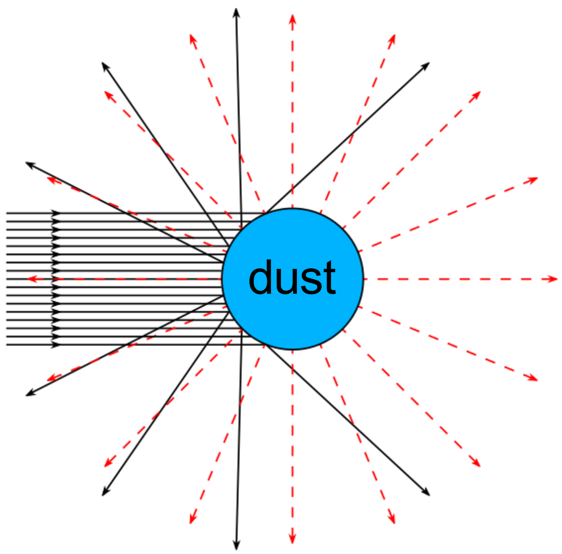

Klacka et al. 2014

Space plasma

velocity vector

(interplanetary) magnetic field

solar wind speed magnitude

(1) $\mathbf{F}_L = q\left(\dot{\mathbf{r}} - \mathbf{u}_{sw}\right) \times \mathbf{B}$

$\mathbf{u}_{sw} = u_{sw}\mathbf{g}_r$

charge

solar wind speed

radial unit vector

Lorentz force:

$$\mathbf{F}_L = q\left(\mathbf{E} + \mathbf{v} \times \mathbf{B}\right) \quad (2)$$

Frozen-in electric field in the solar wind:

$$\mathbf{E} = -\mathbf{u}_{sw} \times \mathbf{B}$$

Transforms (2) into (1)

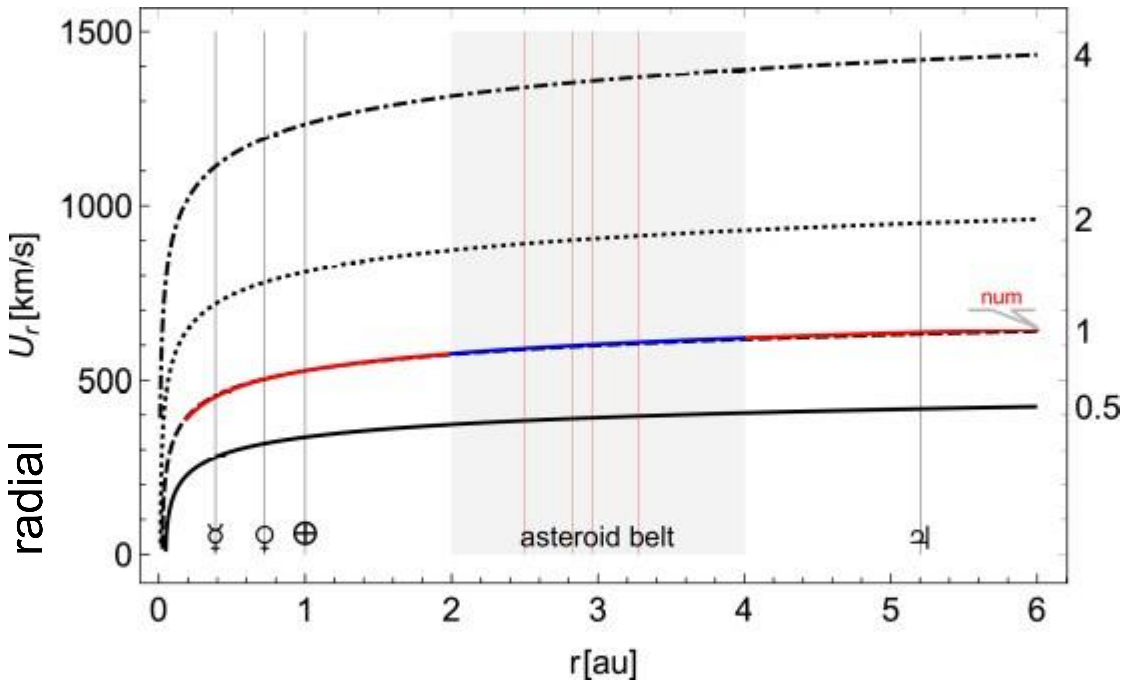

Lhotka & Narita 2019

Lorentz force

background field

charge

reference distance

sun rotation rate

velocity vector

$$\mathbf{F}_L = -\frac{qB_0 r_0^2}{r^2}\left[\frac{1}{r}\mathbf{r}\times\dot{\mathbf{r}} + \frac{\Omega_s}{r}\mathbf{r}\times(\mathbf{r}\times\mathbf{g}_{\tilde{z}}) + \frac{\Omega_s}{u_{sw}}(\mathbf{r}\times\mathbf{g}_{\tilde{z}})\times\dot{\mathbf{r}}\right]\tanh\left(\alpha\frac{\mathbf{r}\cdot\mathbf{g}_{\tilde{z}}}{r}\right)$$

solar distance

solar wind speed

magnetic axis

sign change function

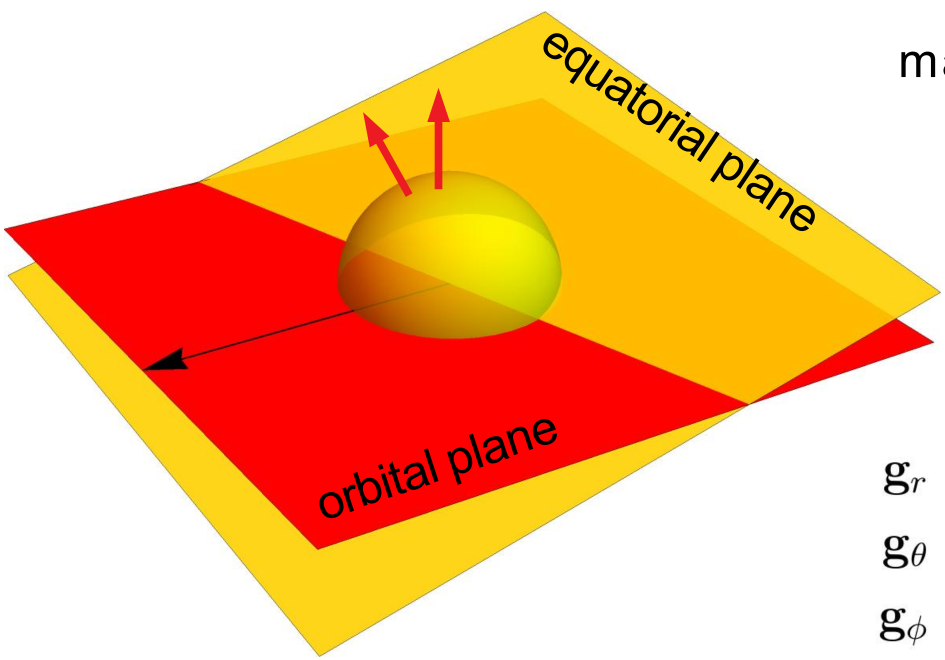

$$\mathbf{B} = \frac{Af(\theta)}{r^2}\left(\mathbf{g}_r - \frac{\Omega_s r \sin(\theta)}{u_{sw}}\mathbf{g}_\phi\right)$$

$$\begin{aligned}
\mathbf{g}_r &= \sin(\theta)\left[\cos(\phi)\,\mathbf{g}_{\tilde{x}} + \sin(\phi)\,\mathbf{g}_{\tilde{y}}\right] + \cos(\theta)\,\mathbf{g}_{\tilde{z}} \,, \\
\mathbf{g}_\theta &= \cos(\theta)\left[\cos(\phi)\,\mathbf{g}_{\tilde{x}} + \sin(\phi)\,\mathbf{g}_{\tilde{y}}\right] - \sin(\theta)\,\mathbf{g}_{\tilde{z}} \,, \\
\mathbf{g}_\phi &= -\sin(\phi)\,\mathbf{g}_{\tilde{x}} + \cos(\phi)\,\mathbf{e}_{\tilde{y}} \,.
\end{aligned}$$

Lhotka & Gales 2019

Space weather and solar activity

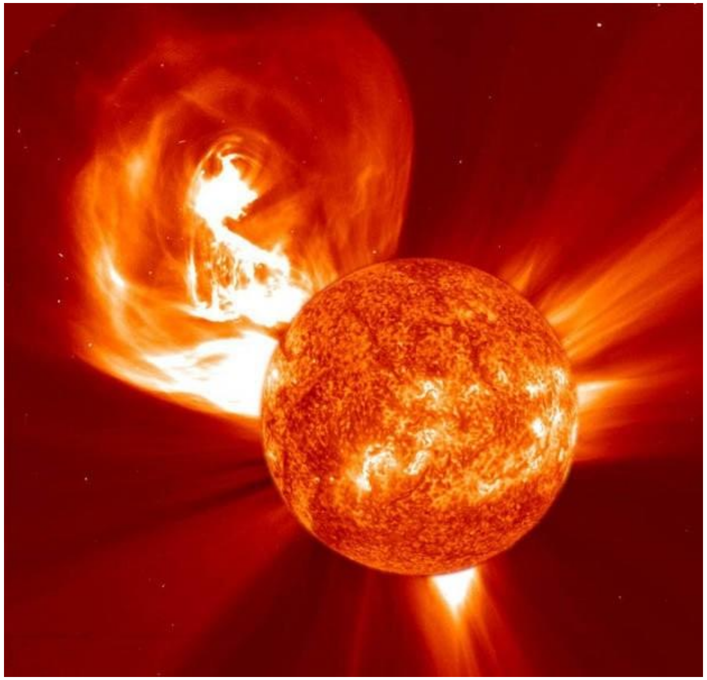

SOHO (NASA and the ESA)

- Source is sun's energy
- Energy released into space in the form of :
  - Light (photons)
  - Atomic particles (ions, electrons, etc..)
  - Magnetic fields
- Typical activity cycles to remember :
  - 27 days (solar rotation period)
  - ~100 days (active region development time scale)
  - Solar cycles : 11 years (22 years, 88 years)
- Heliosphere is the sphere of influence of the sun
- Magnetosphere: created by planetary magnetic fields
  - Deformation by the solar wind
  - Electrons and protons trapped on magnetic field lines

Typical space weather events are:

- X-ray bursts & EUV radiation [8 minutes to reach us]
- Radiation storms (energetic, atomic particles) [15min to 24 hours]
- Geomagnetic storms (triggered by coronal mass ejections that reach the earth) [1-4 days]

Solar wind measurements

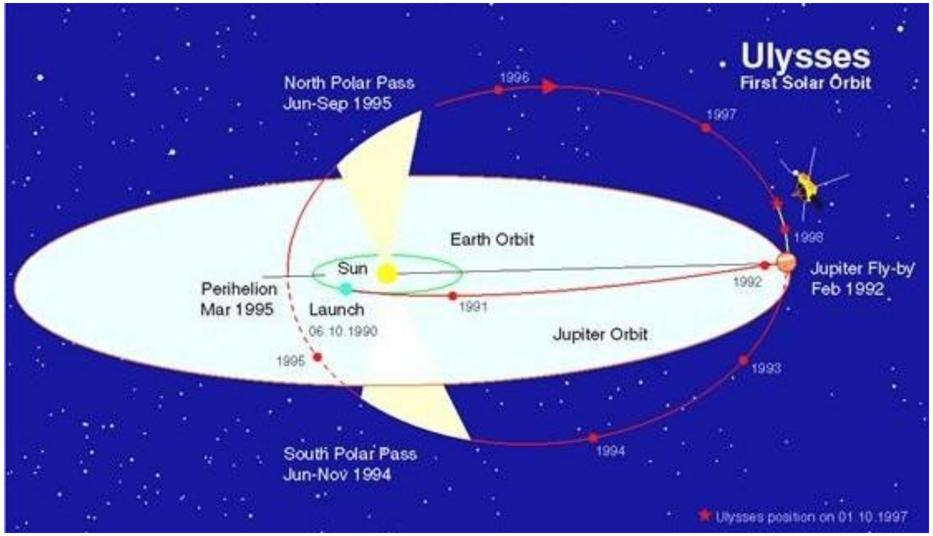

- Ulysses spacecraft with primary mission to orbit the Sun at all (i.e. high) latitudes
- Orbital parameters:
  - a=3.37au (6.2 years orbital period)
  - e=0.6
  - i=80o with respect to Sun's equator
- Launch 1990, 17 years operation
- 3 orbits around the Sun
- Fastest ever flown spacecraft until New Horizons
- Joint mission NASA and ESA

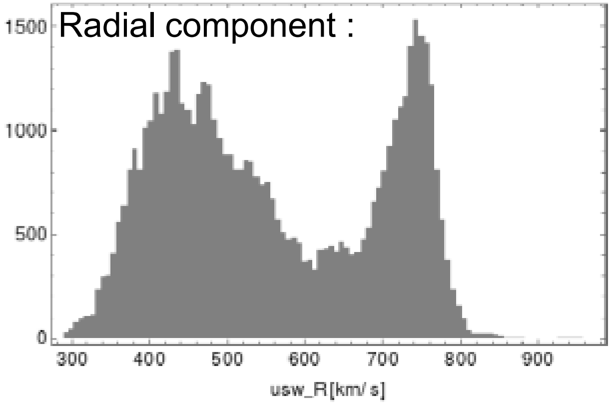

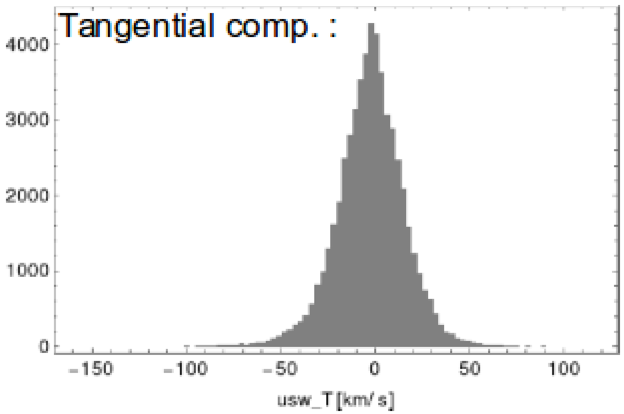

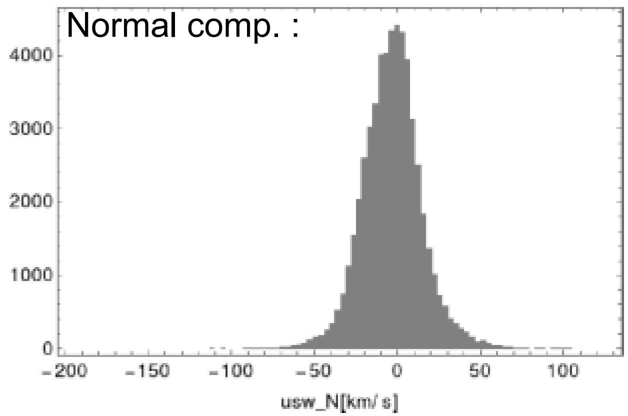

- Variations in density, temperature and speed over time and solar longitude and latitude
- Slow (origin corona) vs. fast (origin coronal holes) solar wind
- Density of slow solar wind = twice density of fsat solar wind

Magnetic field

Radial component :

Tangential comp. :

Normal comp. :

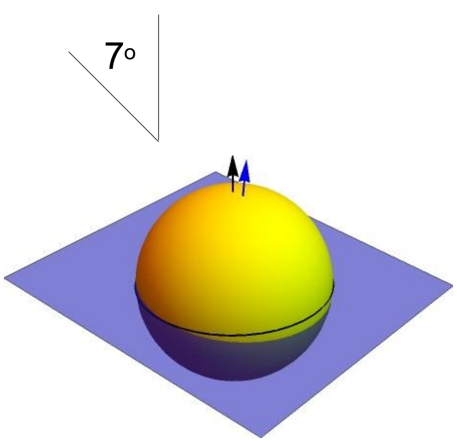

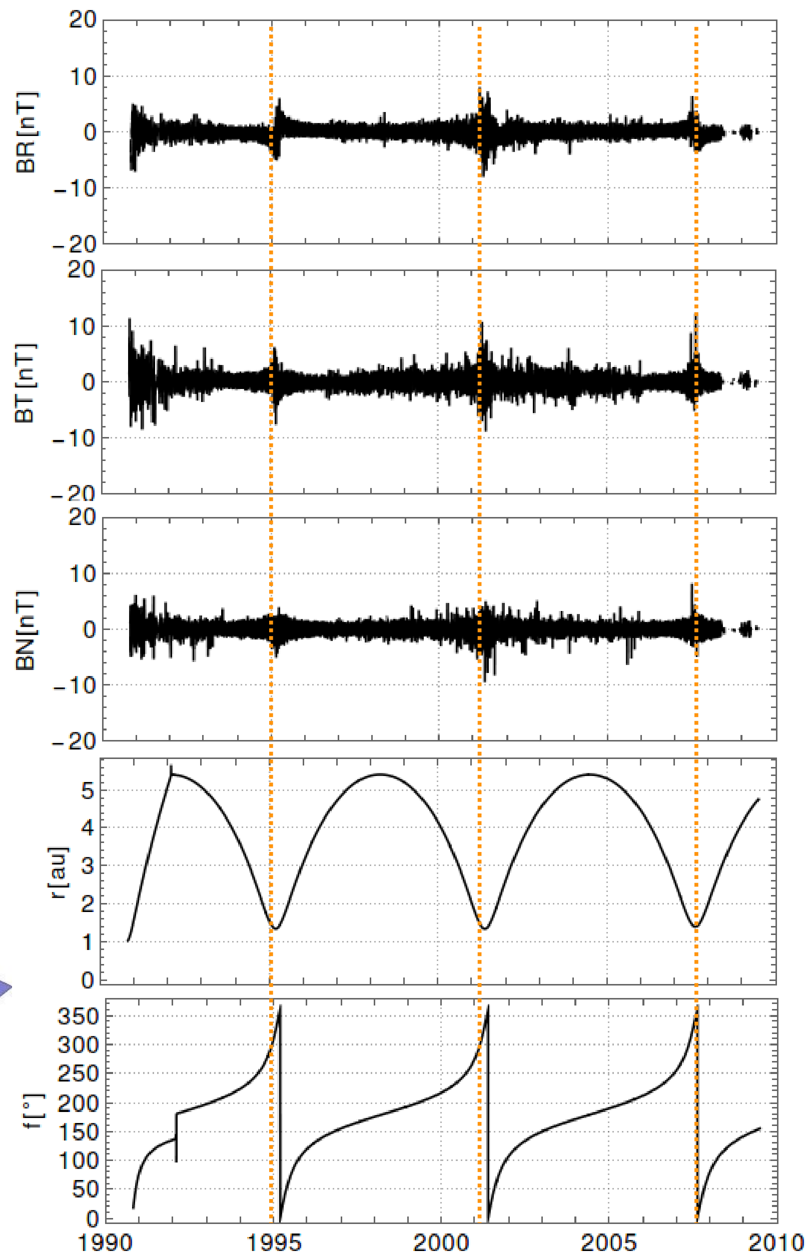

ecliptic

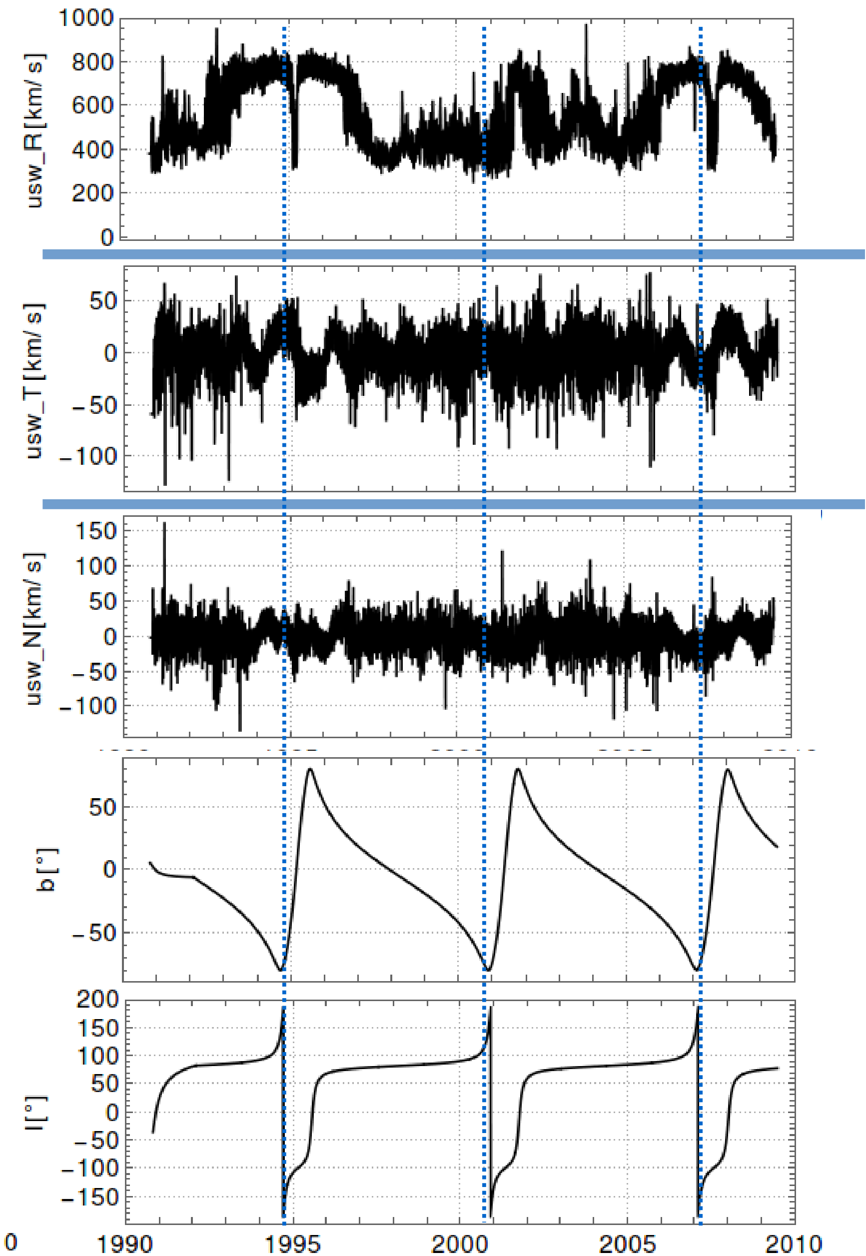

equatorial

Heliospheric field

background field strength

sign change function

sun rotation rate

longitudinal component

$$\mathbf{B} = \frac{A f(\theta)}{r^2}\left(\mathbf{g}_r - \frac{\Omega_s r \sin(\theta)}{u_{sw}}\mathbf{g}_\phi\right)$$

solar distance

radial component

solar wind speed

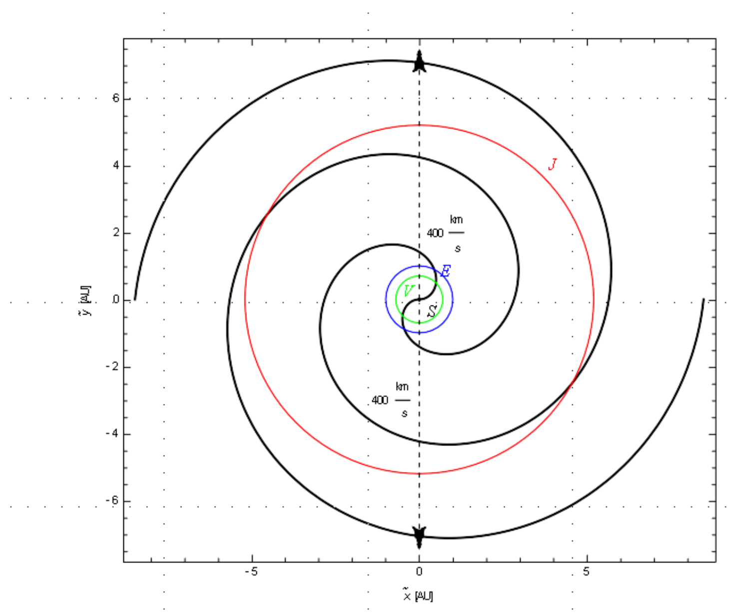

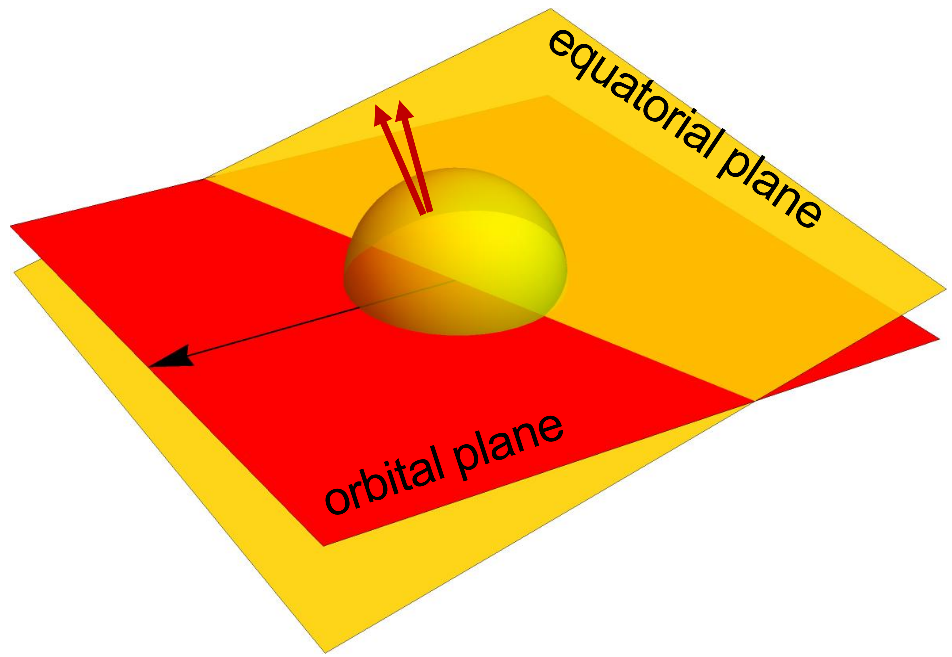

Thermally driven solar wind

Solar gas outflows into interplanetary space (Biermann (1951, 1957) Alfvén (1957))

$$B_R = B_0 \left(\frac{r_0}{r}\right)^2,$$

$$B_T = -r_0 B_0 \left(\frac{r_0}{r}\right) \frac{\Omega_\odot \sin\theta}{U_{sw}}.$$

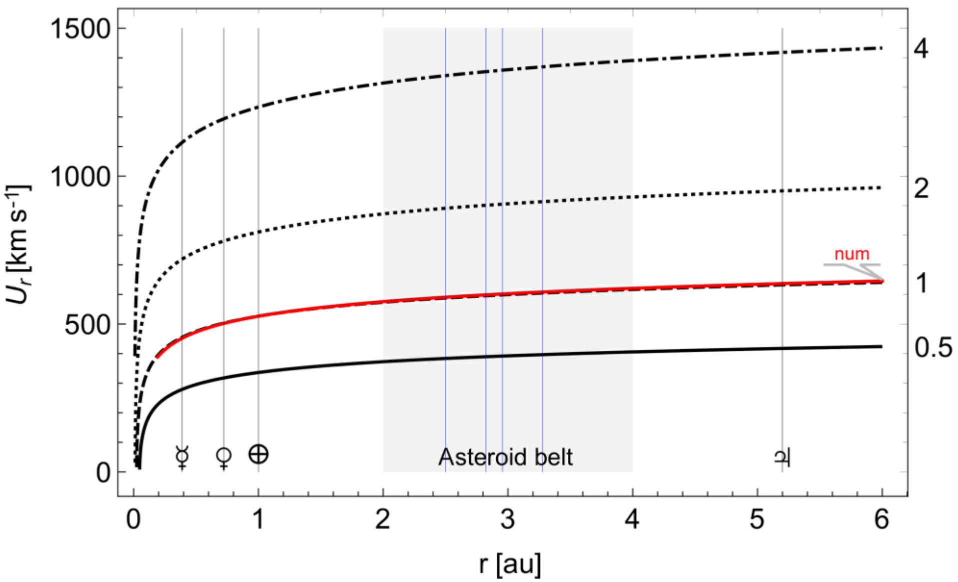

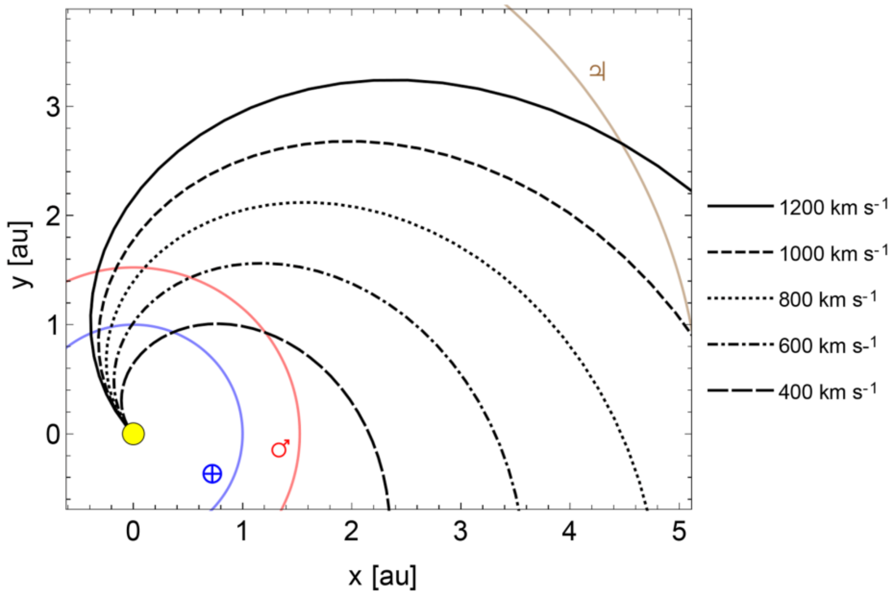

$$U_r \frac{dU_r}{dr} = \left(\frac{2c_s^2}{r} - \frac{GM}{r^2}\right)\left(1 - \frac{c_s^2}{U_r^2}\right)^{-1}.$$

spiral structure of the interplanetary magnetic field (Parker (1958))

Polarity and tilt angle

Polarity of the IMF(inwards and outwards) above and below the current sheet together with the tilt of the solar rotation axis form a wavy current sheet, the so-called ballerina skirt model.

$$B = \frac{A_{\mathrm{mag}}}{r^2}\left(e_r - \Gamma e_\phi\right) \times \left\{1 - 2H\left[\theta - \left(\frac{\pi}{2} + \theta_{\mathrm{tilt}} \sin\left(\phi - \frac{r\Omega_\odot}{U_{\mathrm{sw}}}\right)\right)\right]\right\}$$

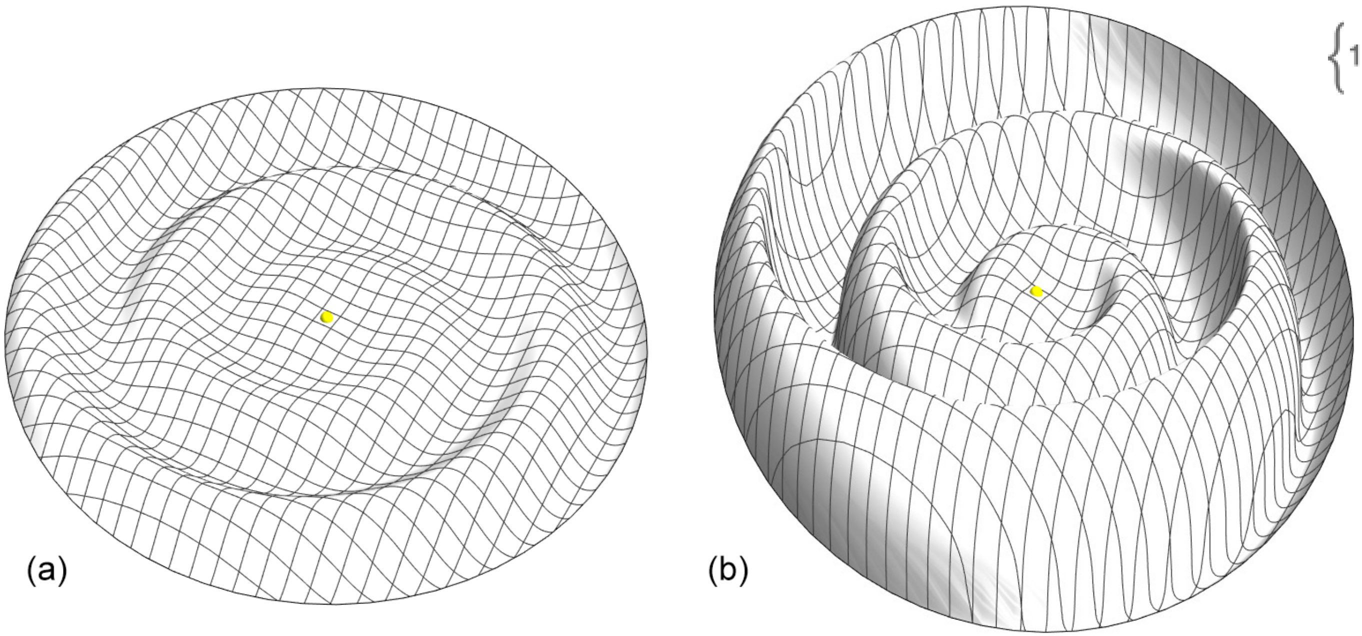

Zero current sheet at given time for slow and fast solar wind conditions (Jokipii and Thomas, 1981)

Presence of magnetic sectors I/II

Sectors become more widely spaced as solar wind speed increases since magnetic field lines become more radial.

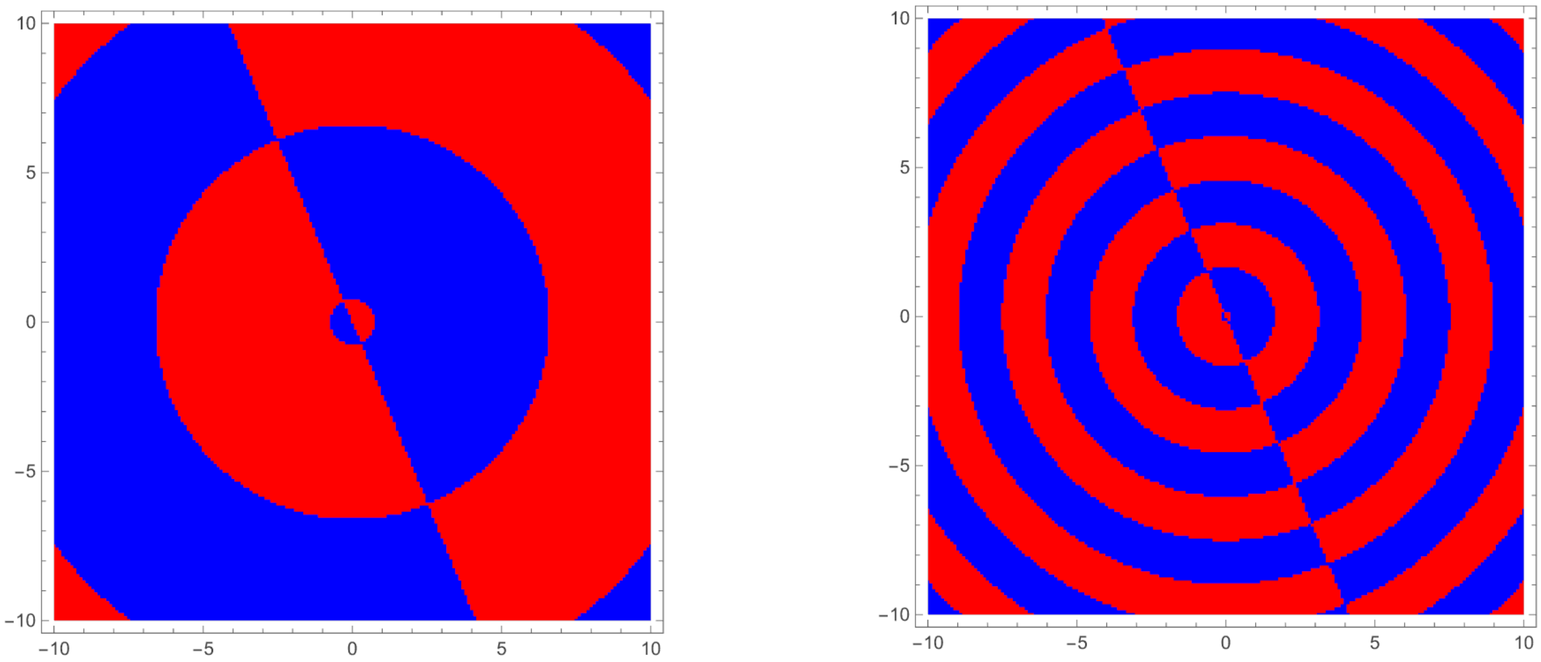

Sectorial structure of the IMF (inwards: blue, outwards: red) within the equatorial plane of the Sun for U=800km/s, vs. 200 km/s (right).

Presence of magnetic sectors II/II

As a consequence of the tilt between the magnetic and rotation axes of the sun a plane that intersects the wavy current sheet contains magnetic sectors.

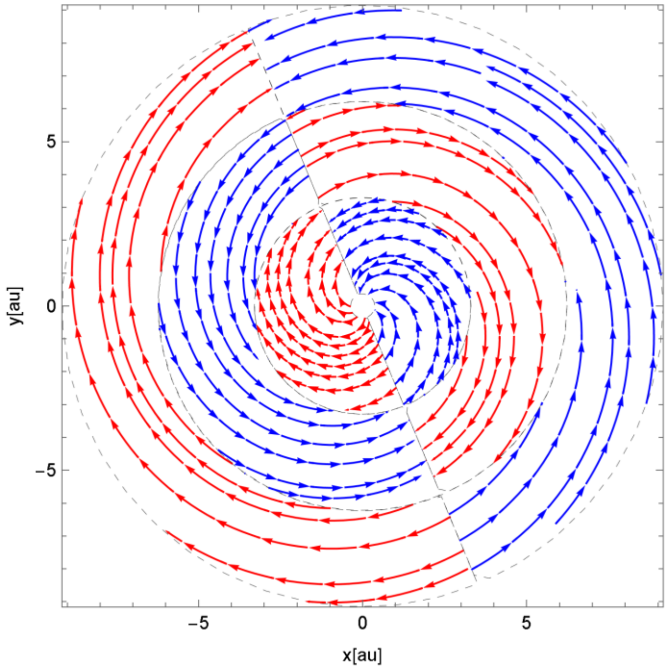

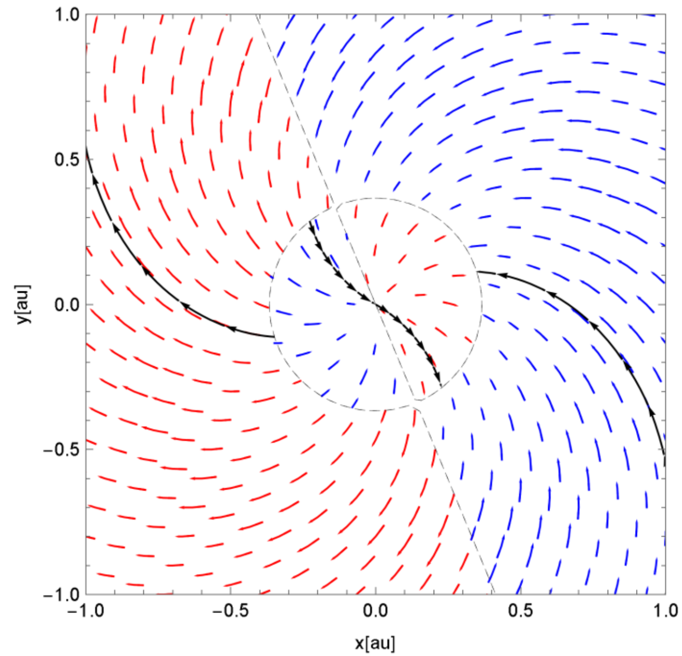

Magnetic field lines (inwards: blue, outwards: red) within the equatorial plane of the sun for U=400km/s, and a tilt angle 5 degrees.

(Lindner Clara 2025)

Everything is time dependent!

Long-Term Trends (Decades to Centuries),
long-term solar magnetic evolution

Solar Cycle (≈11-Year Cycle)
polarity reversal, disordered vs. regular phases

Solar Rotation (≈27-Day Period)
sectorial structure rotates

Transient Events (Minutes to Days)
coronal mass ejections, magnetic clouds

Short-Term Fluctuations (Seconds to Hours),
Alfven waves, turbulence, clocal current sheets

Planetary Interactions (Localized, Time-Variable)
magnetic reconnection

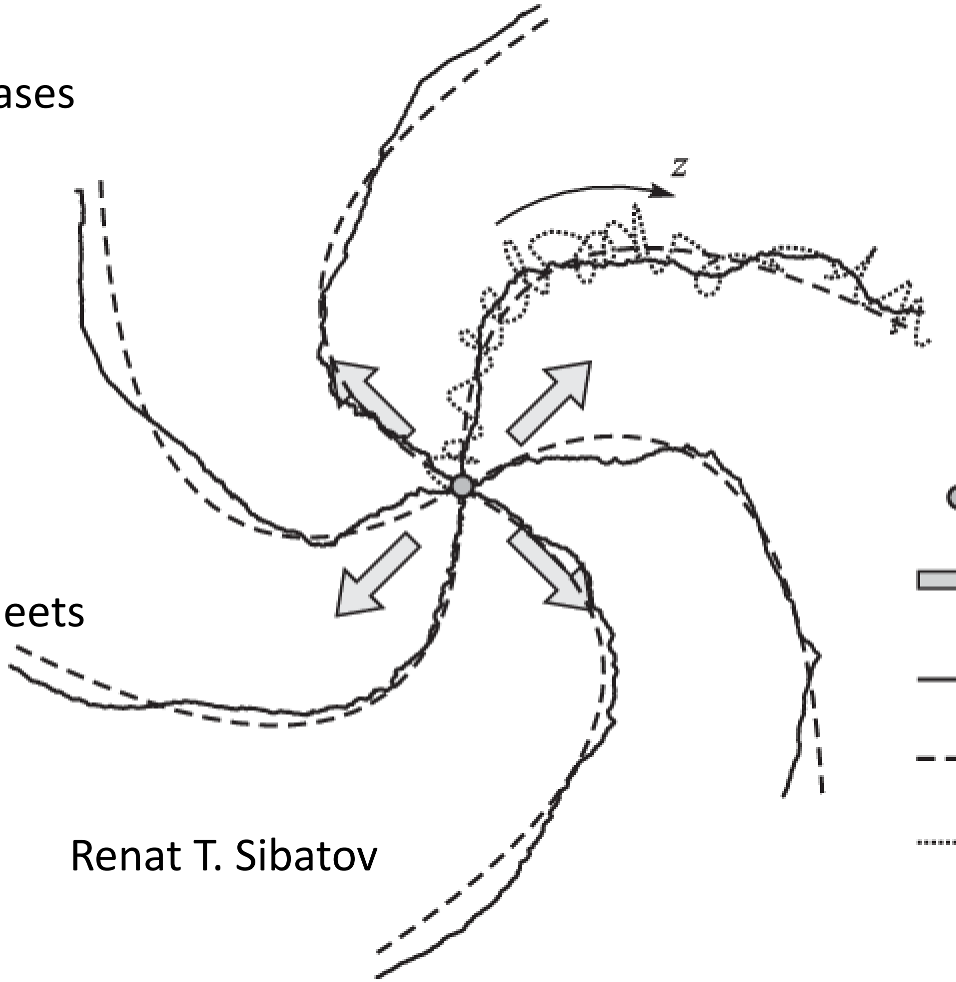

Renat T. Sibatov

Averaged mathematical models

Classical (time dependent) Parker spiral model :

$$B_R = B_0 \left(\frac{r_0}{r}\right)^2 b_R(t) \qquad b_R(t) = \cos\left(2\pi t/T + \varphi_0\right)$$

$$B_T = B_0 \left(\frac{r_0}{r}\right) b_T(t) \qquad b_T(t) = \cos(\vartheta) \cos\left(2\pi t/T + \varphi_0\right)$$

Importance of the normal component :

$$B_N = B_0 \left(\frac{r_0}{r}\right)^\kappa b_N(t) \qquad b_N(t) = 1 + \cos\left(2\pi t/T\right)$$

Study in distance for different κ (1=black, 2=red, 3=blue) :

- Mimics solar cycle with period T
- Radial component falls with $1/r^2$
- Tangential component falls with $1/r$
- Normal component falls with $1/r^\kappa$
- Non-zero mean of normal component

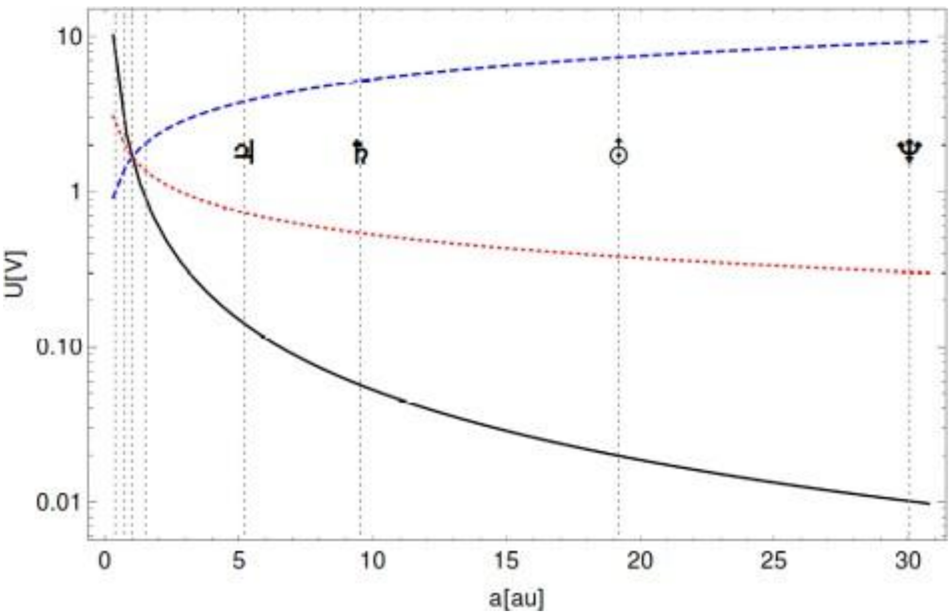

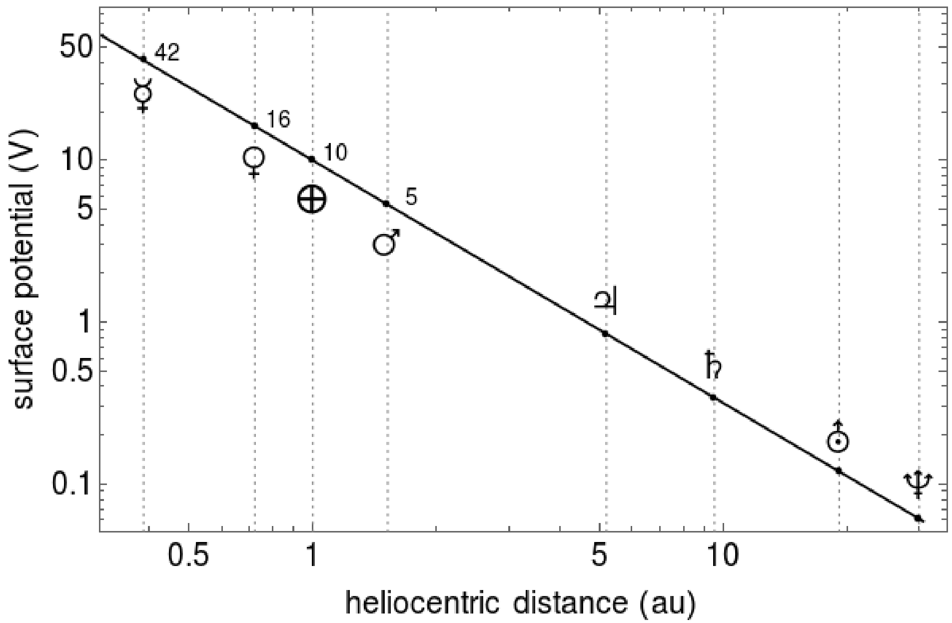

Dynamical effects on radial distance

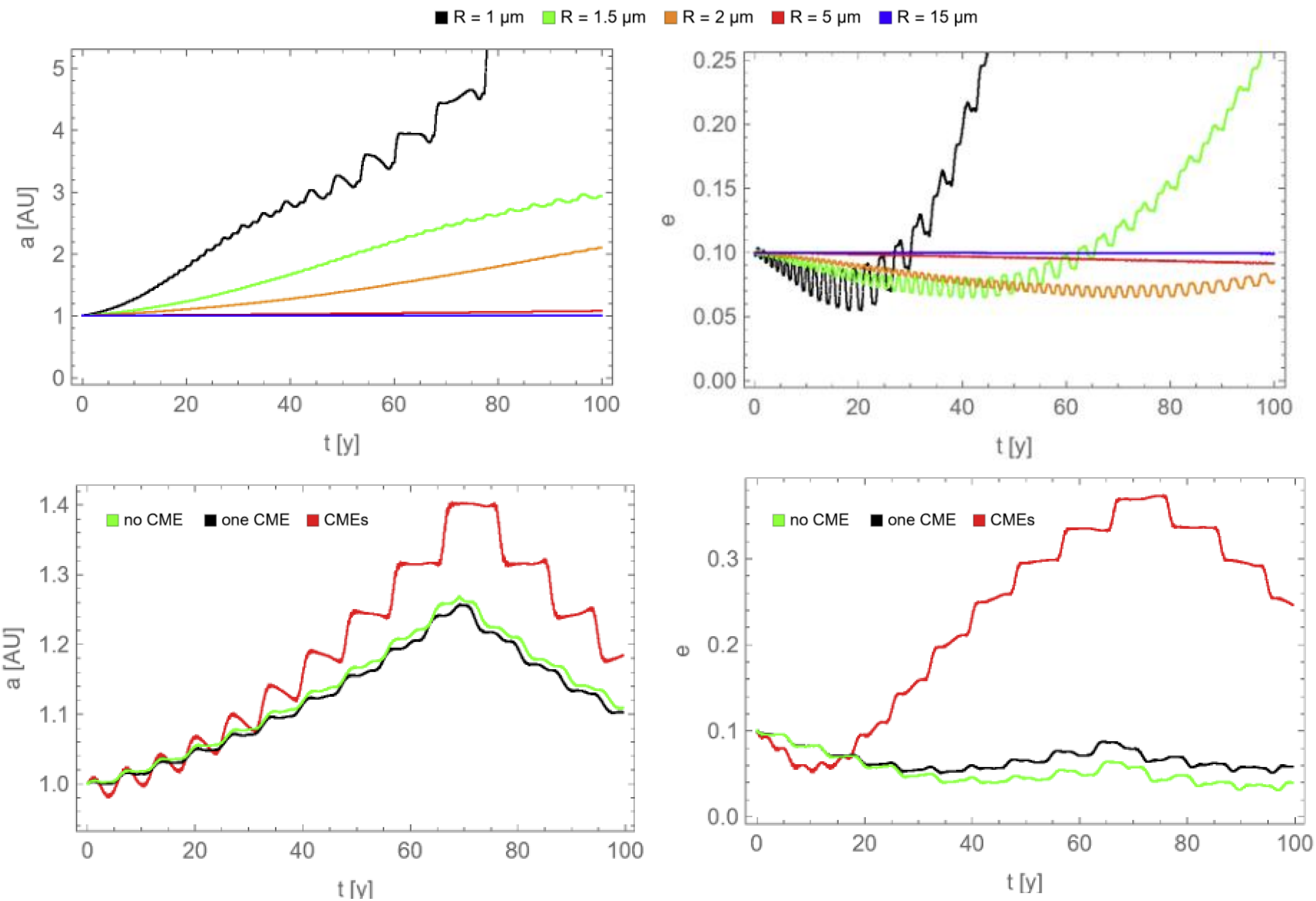

Latitudinal (spatial) dynamics

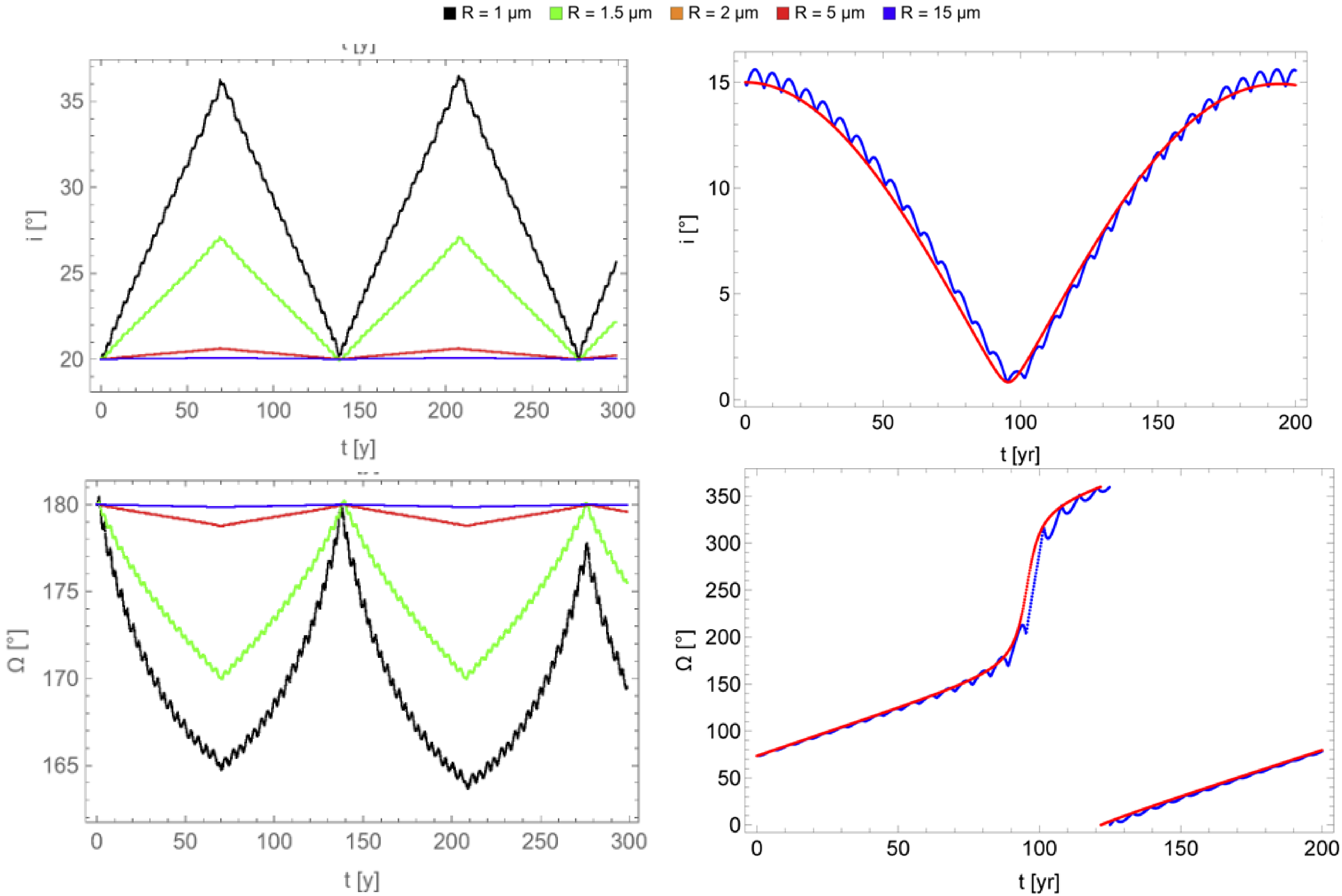

Secular dynamics I/II

- Drift depending on sign of charge.
- 'Seasonal' component with period of 22 years
- Stochastic component un-modeled

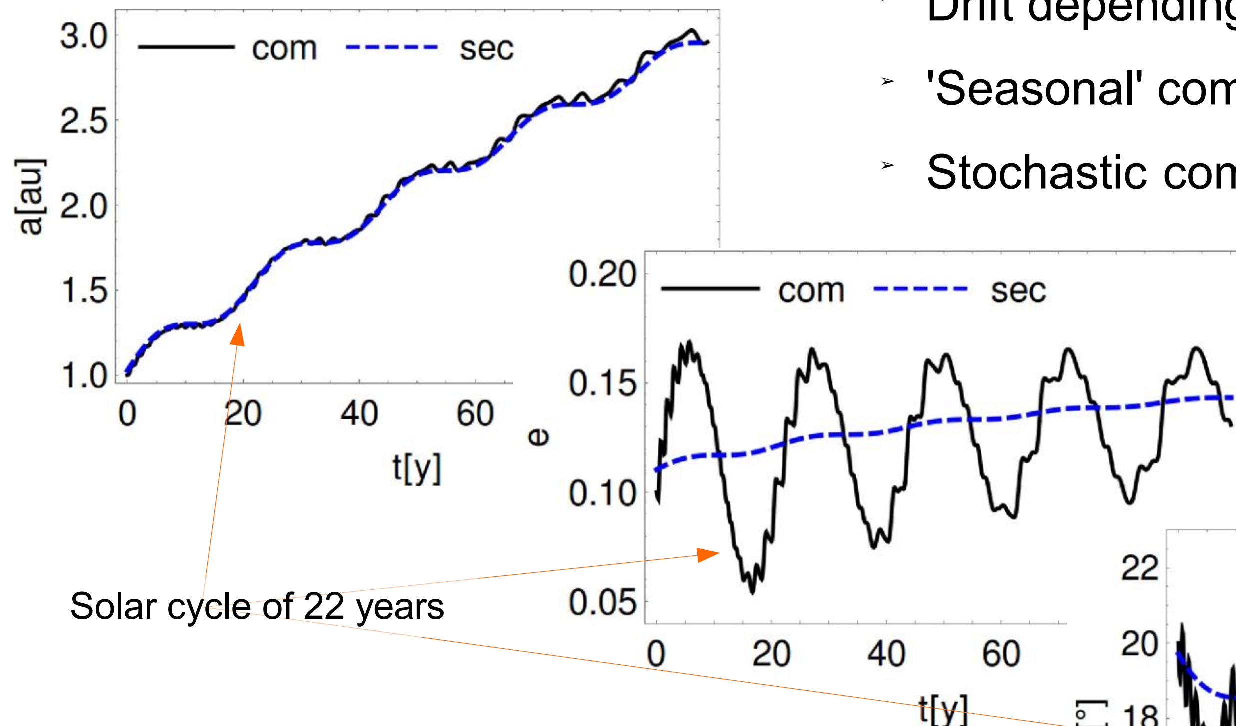

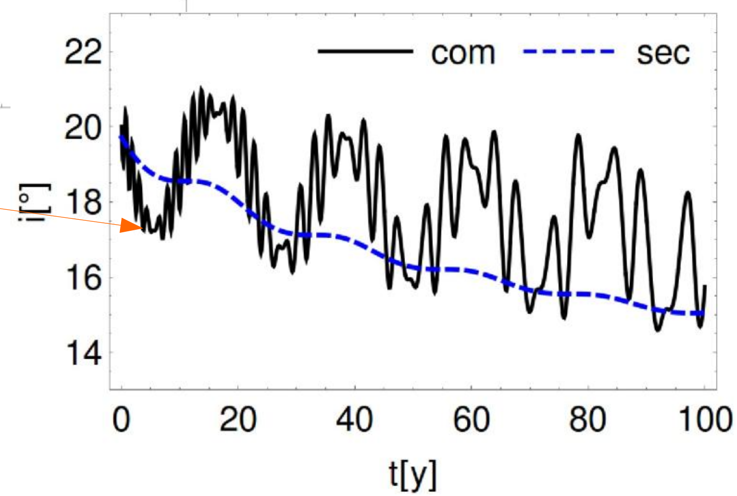

Background magnetic field strength $3\mathrm{nT}$ at $1\mathrm{au}$.
particle $1\mu\mathrm{m}$, density $2\mathrm{g/cm^3}$, potential $5\mathrm{V}$.

Lhotka, Bourdin, Yasuhito (2016)

Secular dynamics II/II

Secular orbital evolution influenced by:

- Deviation between magnetic axis and rotation axis : ω_3
- Norm of the normal magnetic field component : B_N
- Reciprocal of semi-major axis : $1/a^\kappa$

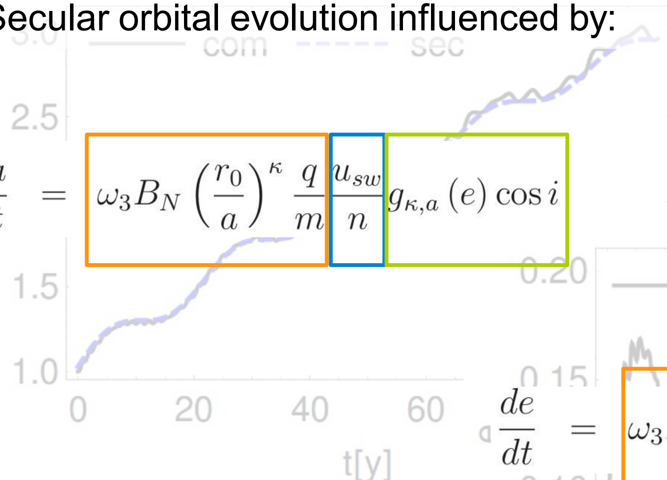

$$\frac{da}{dt} = \boxed{\omega_3 B_N \left(\frac{r_0}{a}\right)^\kappa \frac{q}{m}}\boxed{\frac{u_{sw}}{n}}\boxed{g_{\kappa,a}(e)\cos i}$$

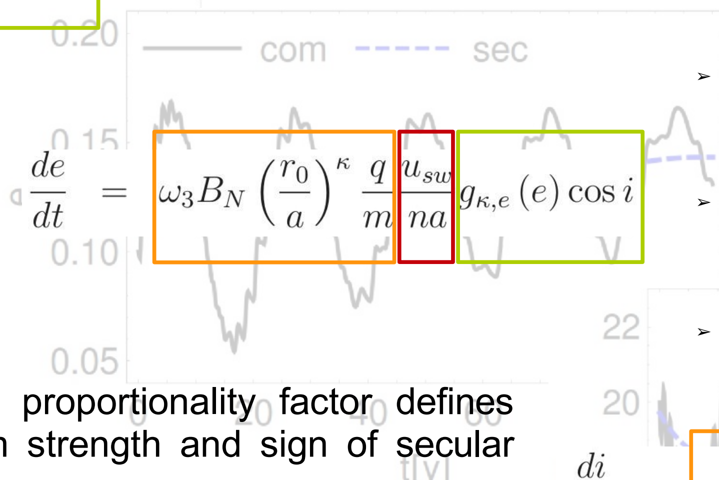

$$\frac{de}{dt} = \boxed{\omega_3 B_N \left(\frac{r_0}{a}\right)^\kappa \frac{q}{m}}\boxed{\frac{u_{sw}}{na}}\boxed{g_{\kappa,e}(e)\cos i}$$

- Charge over mass ratio: q/m (sign!)
- Ratio of solar wind speed over mean motion u_{sw}/n
- Orbit geometry : e,i

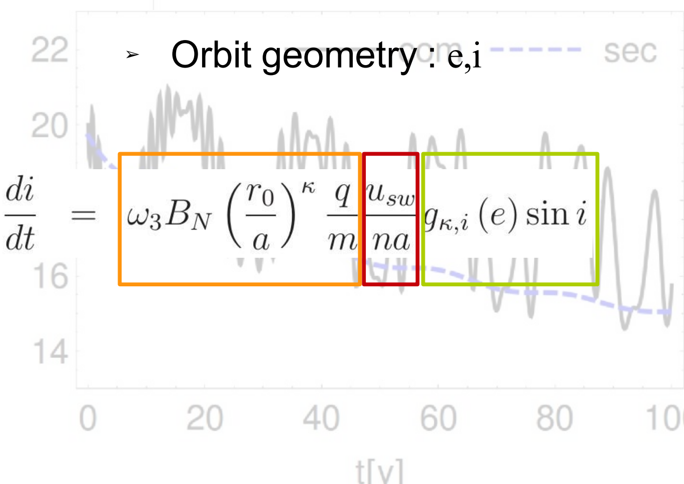

$$\frac{di}{dt} = \boxed{\omega_3 B_N \left(\frac{r_0}{a}\right)^\kappa \frac{q}{m}}\boxed{\frac{u_{sw}}{na}}\boxed{g_{\kappa,i}(e)\sin i}$$

$\boxed{\omega_3 B_N \left(\frac{r_0}{a}\right)^\kappa \frac{q}{m}}$

- Common proportionality factor defines maximum strength and sign of secular drift

$\boxed{\frac{u_{sw}}{n}}$ vs. $\boxed{\frac{u_{sw}}{na}}$

- Additional 1/a factor decreases effect for eccentricity and inclination
- Secular effects decrease / increase for increasing inclination

Lhotka, Bourdin, Yasuhito (2016)

Balanced (stable) solutions

Dependency on solar wind conditions
normal magnetic field strength
solar radiation pressure

- Inverse proportional to mean solar wind speed
- Inverse proportional to mean normal interplanetary magnetic field component
- Direct proportional to ratio of solar radiation pressure of gravitational attraction of the Sun

$$\frac{q}{m}=\frac{\boxed{\beta}}{c}\frac{(Q+\eta)}{\boxed{Q}}\frac{n^{3}a^{\kappa+2}G_{\kappa}(e)}{r_{0}^{\kappa}\cos(i)}\left(\boxed{B_{N}}\boxed{u_{sw}}\omega_{3}\right)^{-1}$$

Dependency on optical parameters :

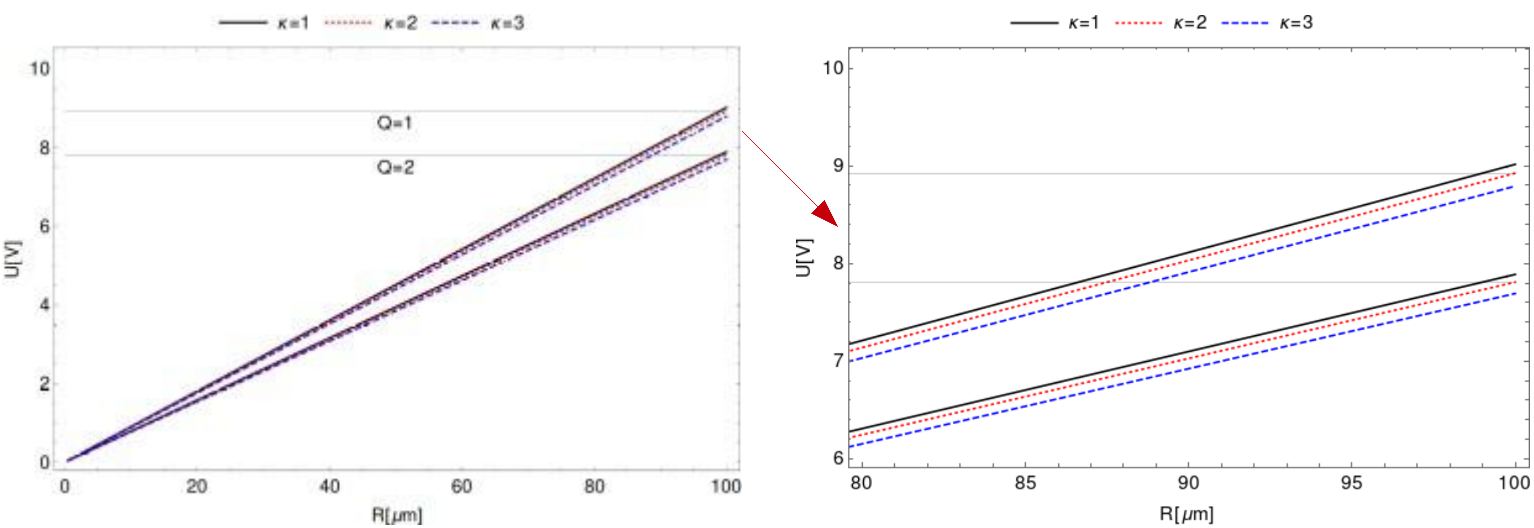

Different IMF models

Different optical and physical properties

Dependency on physical parameters :

- Depends on optical efficiency factor Q (incoming vs. outgoing vs. absorbed energy in photon – particle interaction)
- Depends on particle size and density of the dust grain
- Charging mechanisms, stability of charge equilibrium

Resonant capture I/III

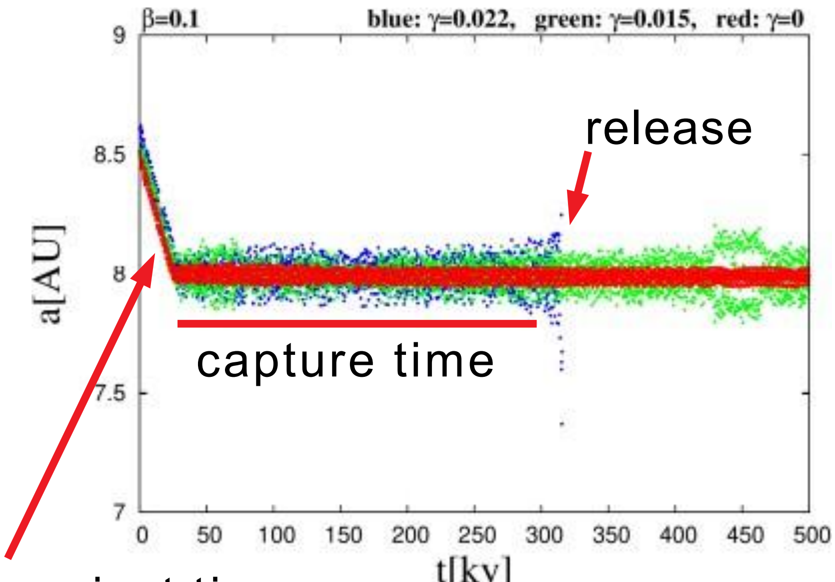

Transient time

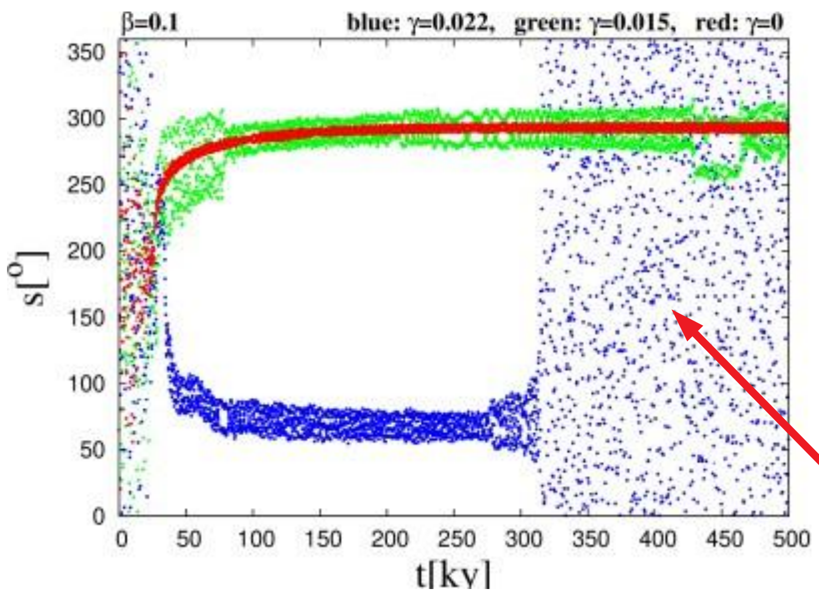

out of resonance

Color code :

Lhotka & Gales 2019

- red = uncharged
- green = slightly charged
- blue = higher charge

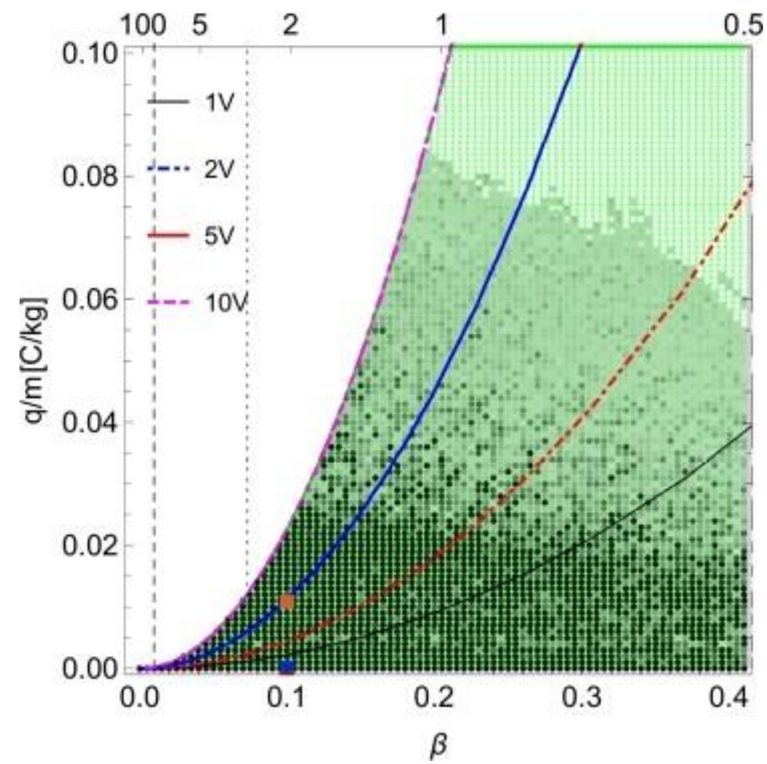

Resonant capture II/III

resonant argument: $qs = (p+q)\lambda_1 - p\lambda + q\bar{\omega}$

Lhotka & Gales 2019

Gravitational problem :

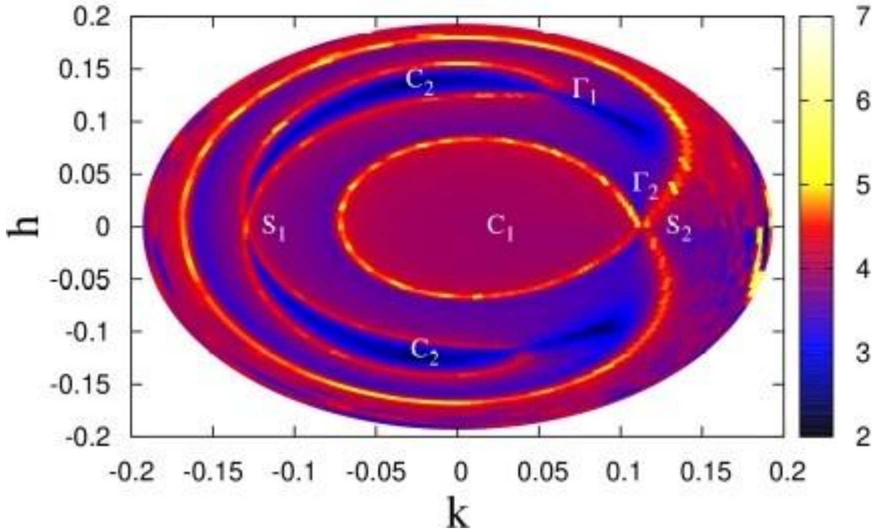

Gravity + Lorentz force

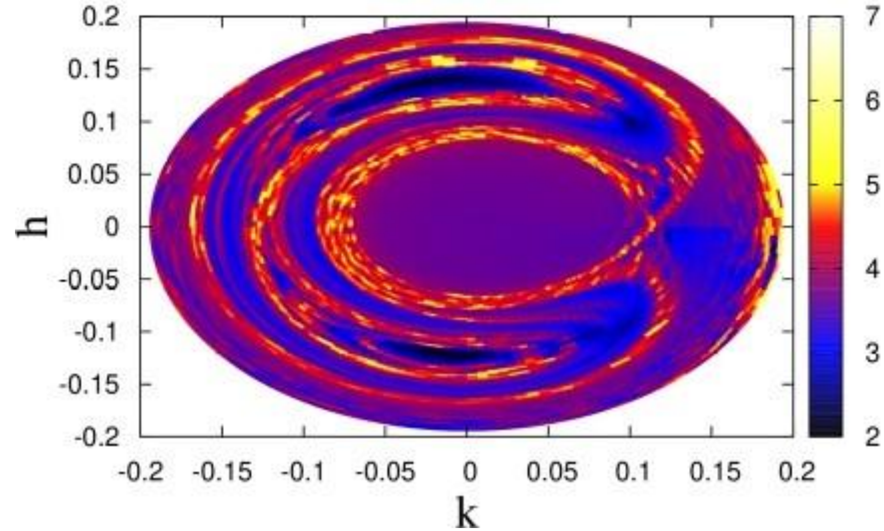

S_1, S_2 : saddles of the resonance
Γ_1, Γ_2 : separatrices
C_1, C_2 : bounded regions

$$(k,h) = (e\cos(s), e\sin(s))$$

eccentricity resonant argument:

Charge 'blurs' widths of separatrix curves.

Resonant capture III/III

On short time scales motion is trapped in specific regions:

- librational motion :
  - red, green (tadpole type)
  - yellow, black (horseshoe type)
- rotational motion :
  - magenta (small eccentricites)
  - cyan (large eccentricities)

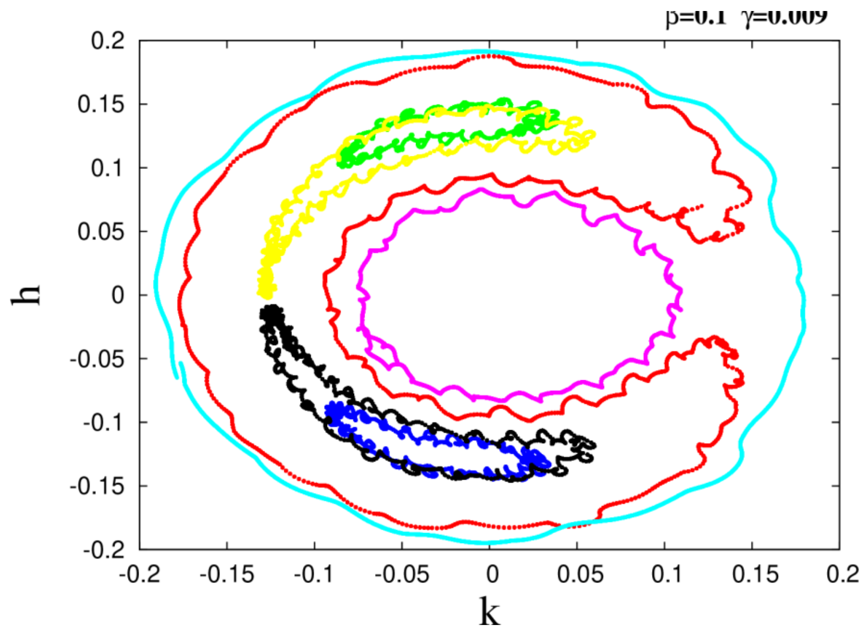

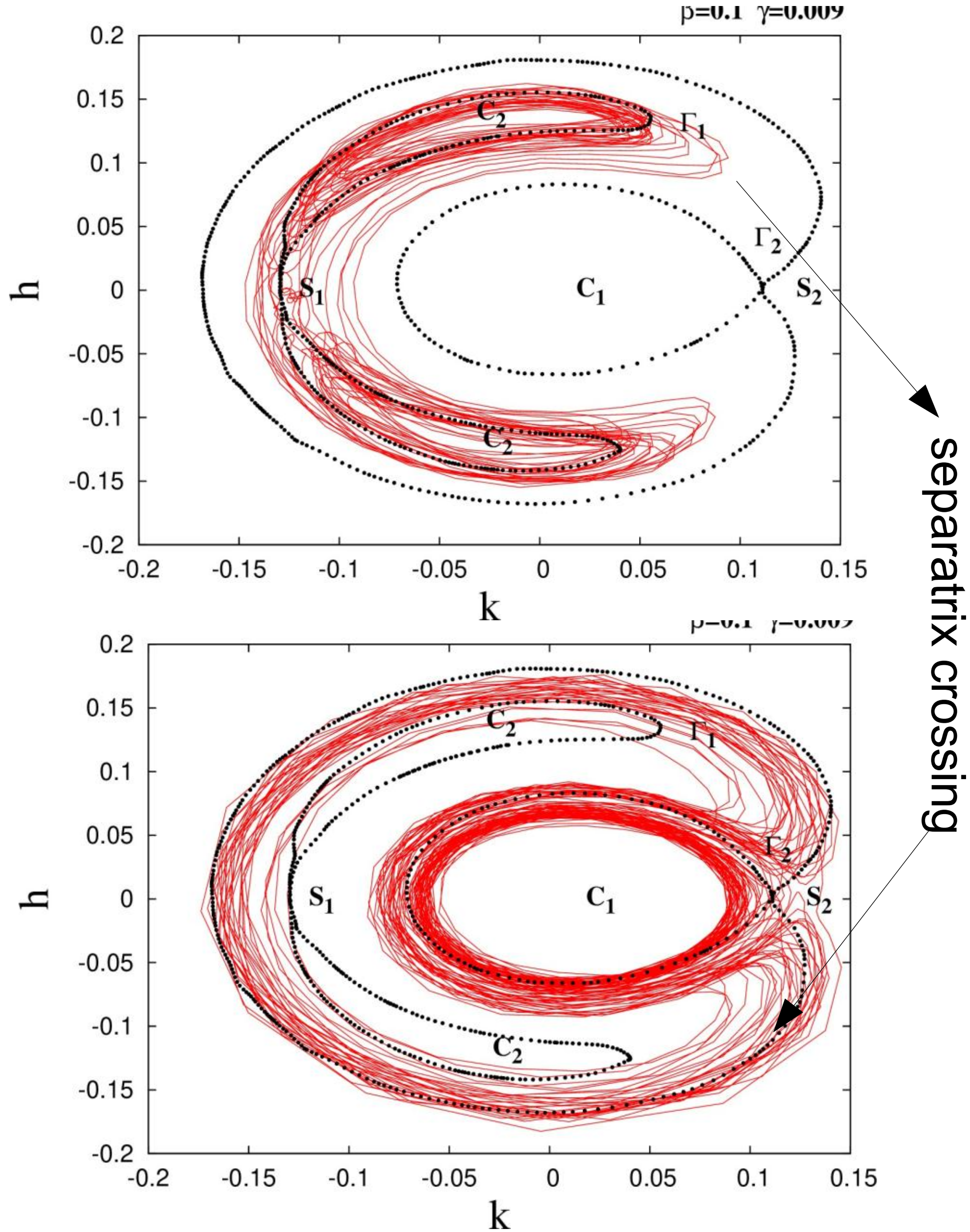

Co-orbital motions

Dvorak, Lhotka 2013

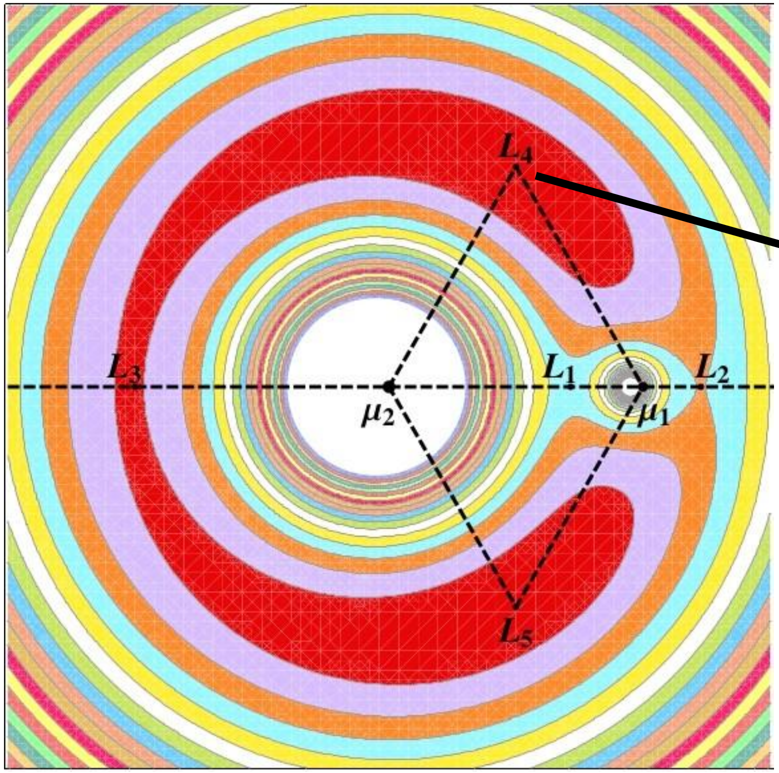

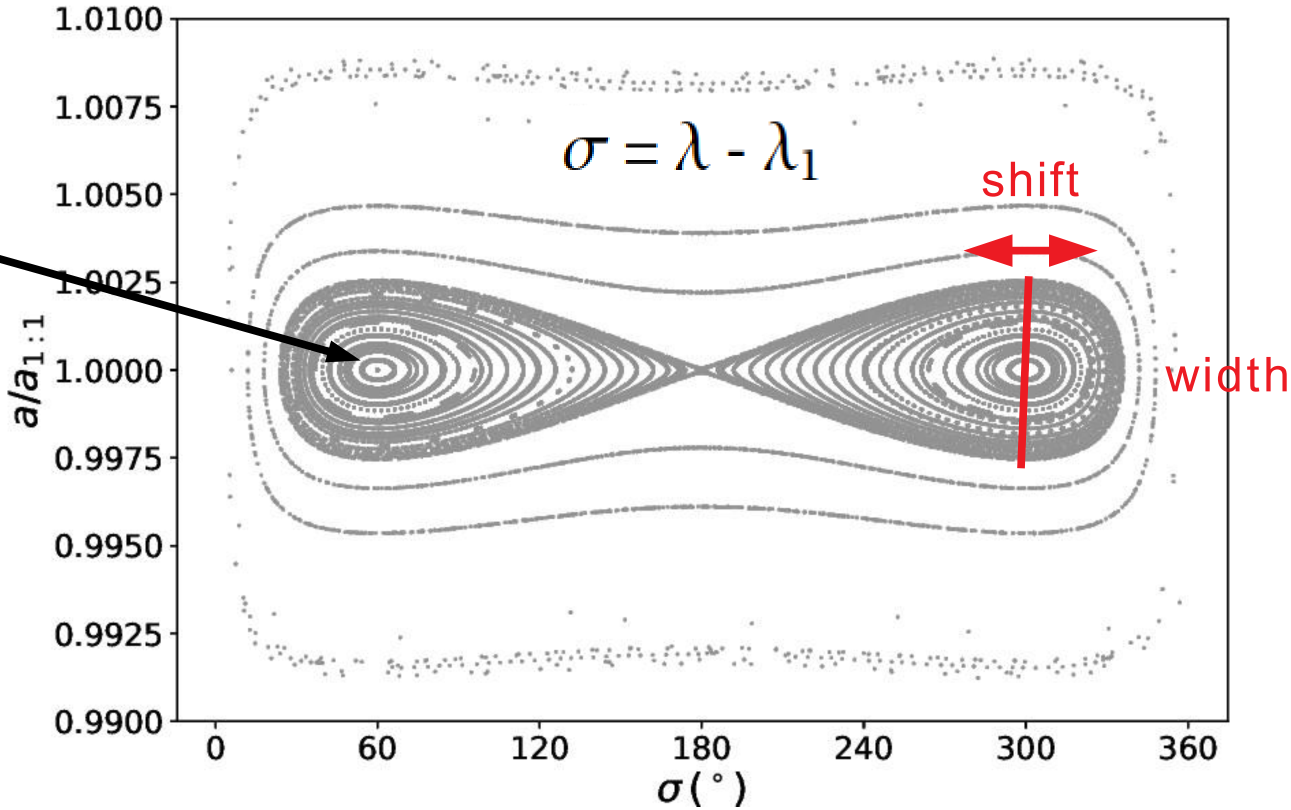

- Lagrange problem: 1:1 MMR between planet (Jupiter, Venus, etc…) and dust particle.

- Particles near L4, L5 experience temporary capture

- Strong influence of non-gravitational forces on location / resonance width / capture times

Shift of equilibria I/II

Poynting-Robertson effect and solar wind drag on resonant motion close to L_4 (1:1):

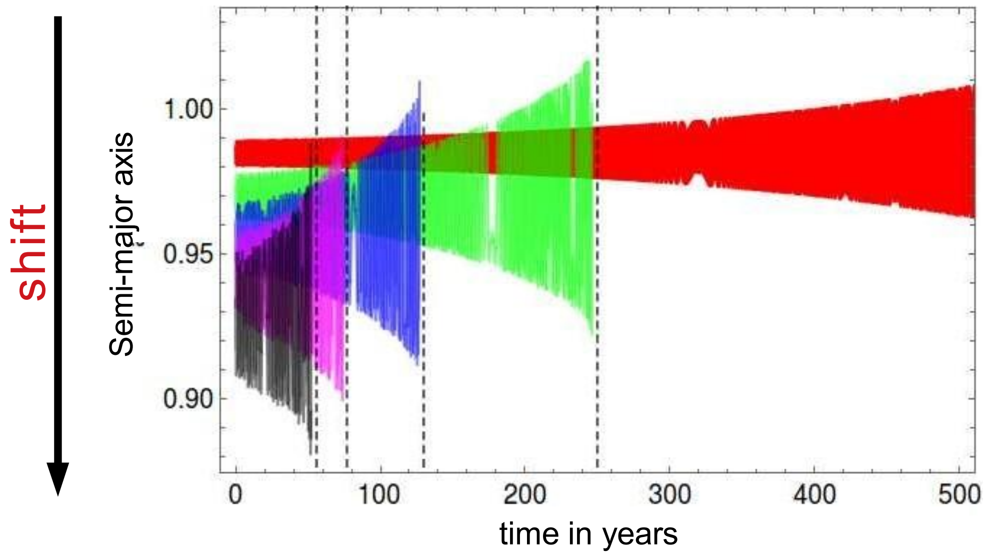

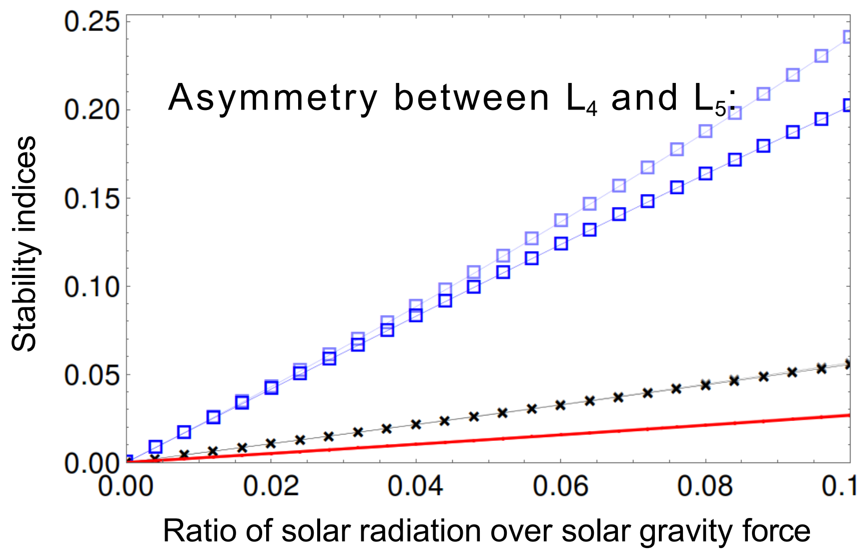

Temporary capture for different size-to-mass ratios between primary and secondary

The higher the size-to-mass ratio the shorter the time of temporary capture.

Analysis of stability indices reveal instability of motion close to resonance.

Depending on the physical parameters solar wind induces an asymmetry of the symmetric problem in the pure gravitational case.

Lhotka & Celletti 2015

Shift of equilibria II/II

Influence of non-gravitational forces on location of exact resonance condition

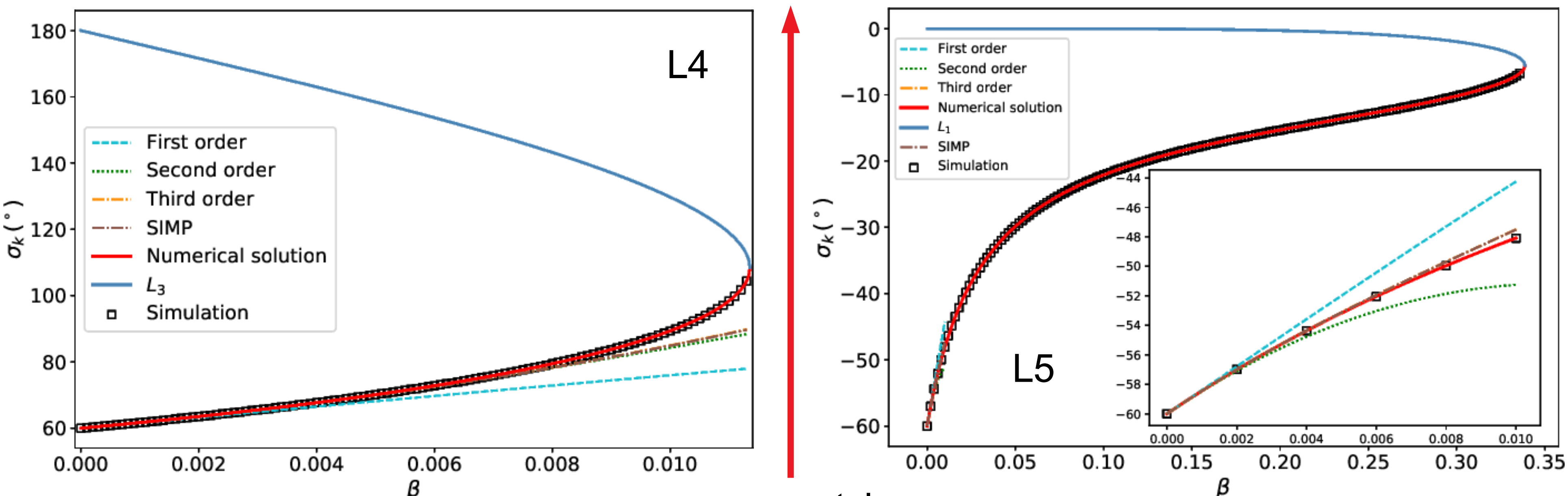

asymmetric

Zhou et al. 2021

- Asymmetry is caused by Poynting-Robertson effect and solar wind drag

- Strong dependency on size and composition (parameter beta)

- Does not only affect location of equilibria – but also resonance widths…

Extent of resonance widths

Non-gravitational forces play a crucial role in the extent of the resonance widths:

- Strong dependence on particle radii

- Symmetry between L4 and L5 is broken for micron sized dust grains

- Probability of temporary trapping close to L4 smaller compared to L5

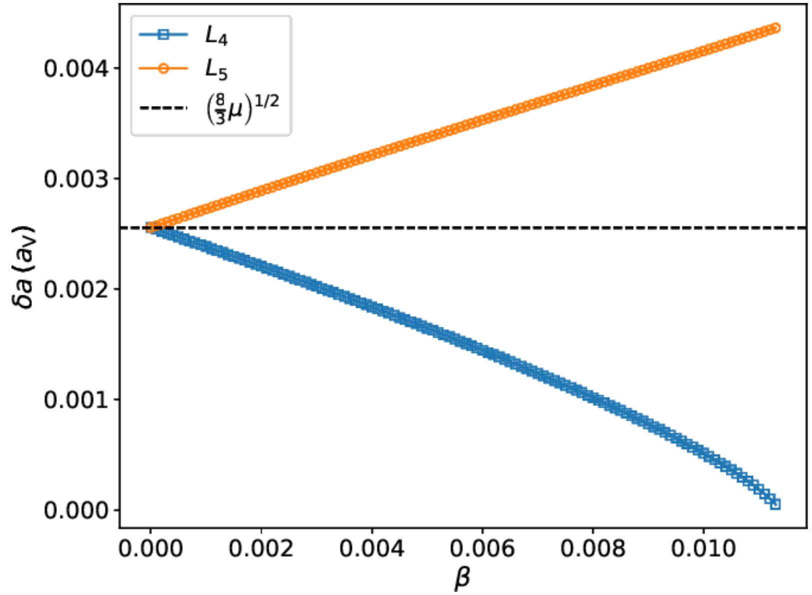

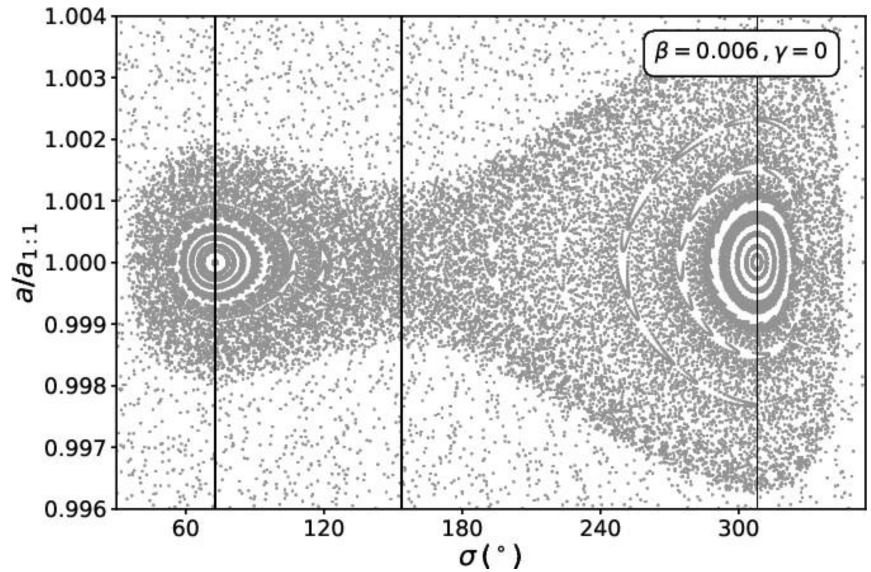

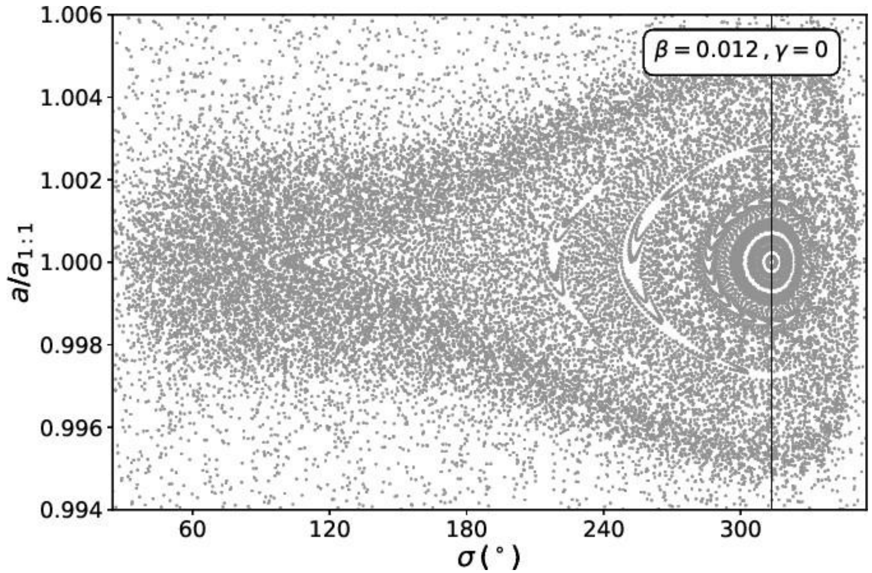

Temporary capture times

Capture times for dust grains are different in the inner / outer solar system.

Co-orbital with Jupiter

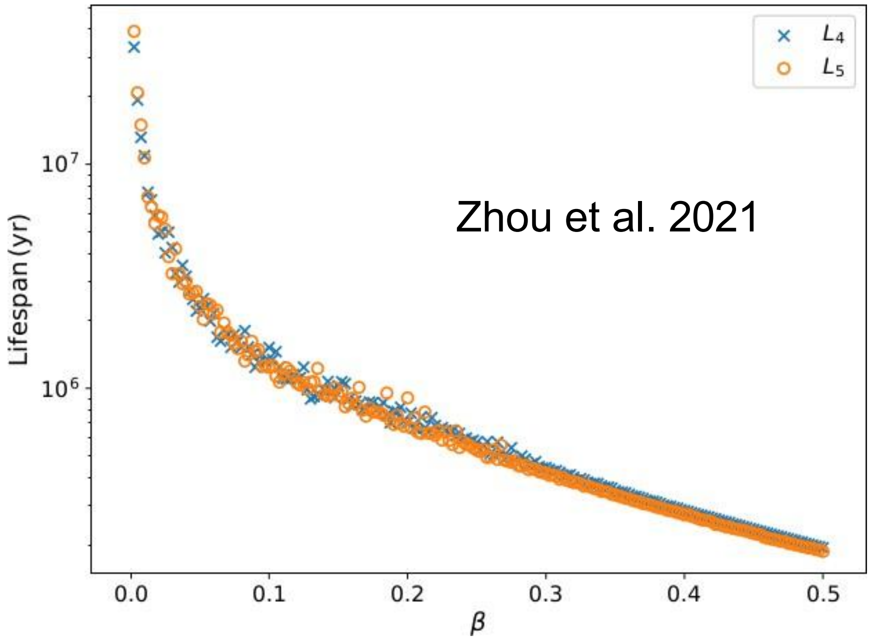

Co-orbital with Venus

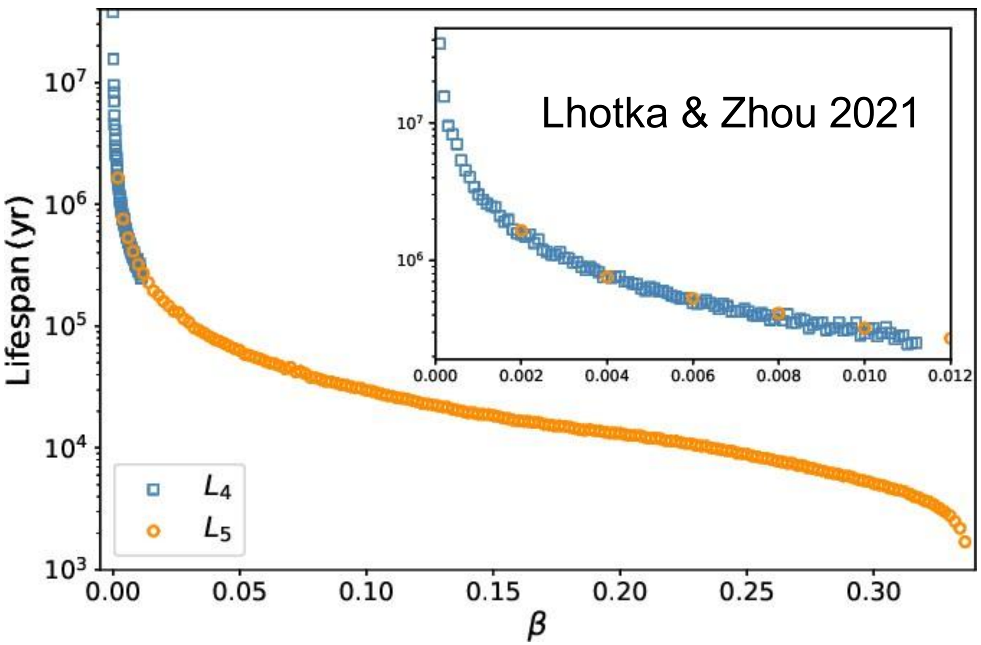

Structure of the curves depends on:

- distance from the sun (inner vs. outer solar system)
- particle size (radius, size-to-mass ratio)
- mass of the co-orbital planet (Venus vs. Jupiter)

Specific role of charge I/III

- Release from resonant locking occurs on shorter time scales.

- The resonant regions get distorted and shifted due to the interaction with the interplanetary magnetic field.

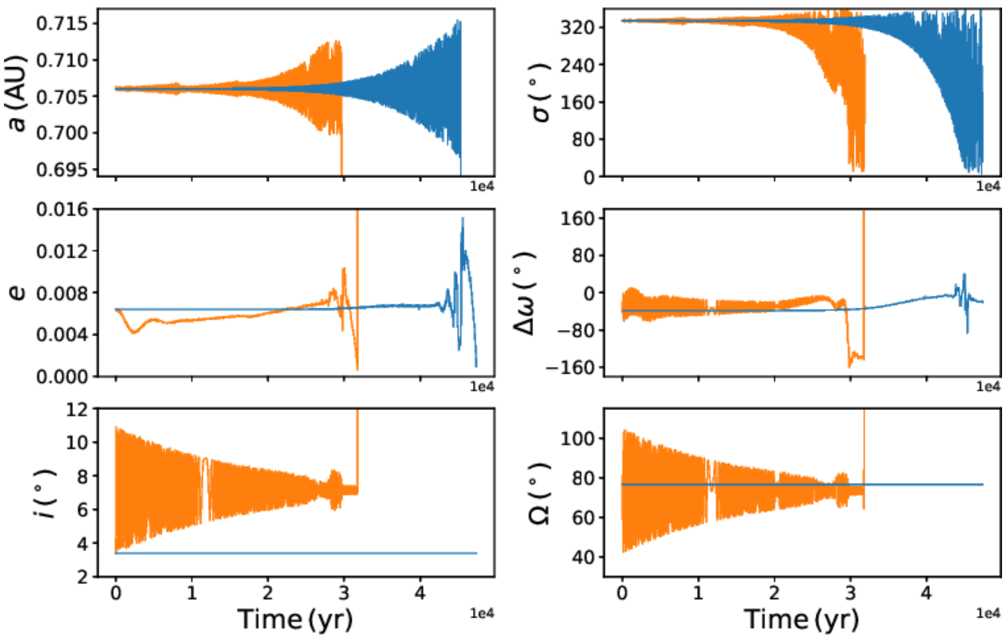

Reduced capture times: temporary capture of uncharged (blue) and charged (orange) particles.

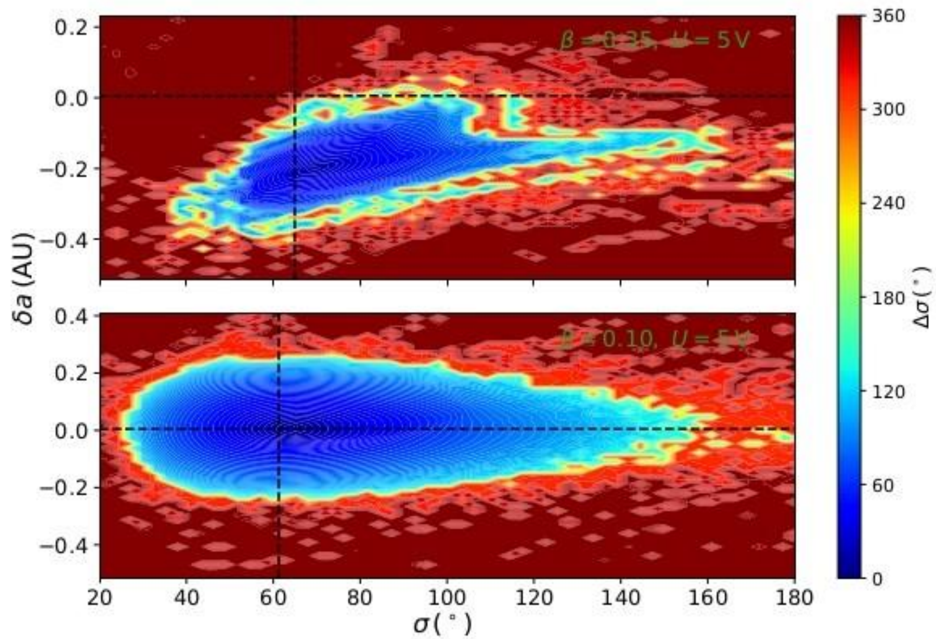

Libration amplitudes around resonant values in presence of charge.

Lhotka & Zhou 2021

Specific role of charge II/III

Capture in resonant lock in mean motions with planet Jupiter (outer solar system).

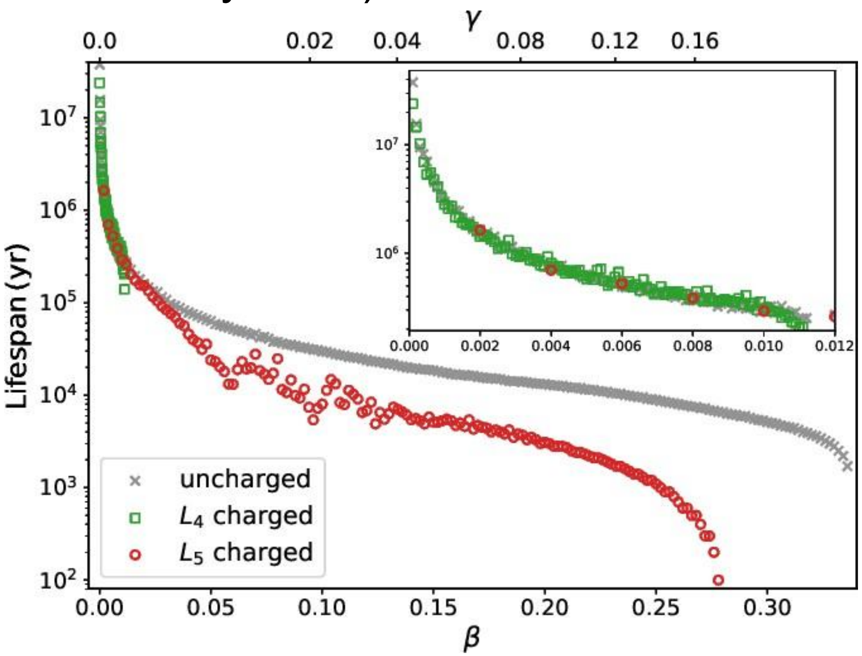

Capture in resonant lock in mean motions with planet Venus (inner solar system).

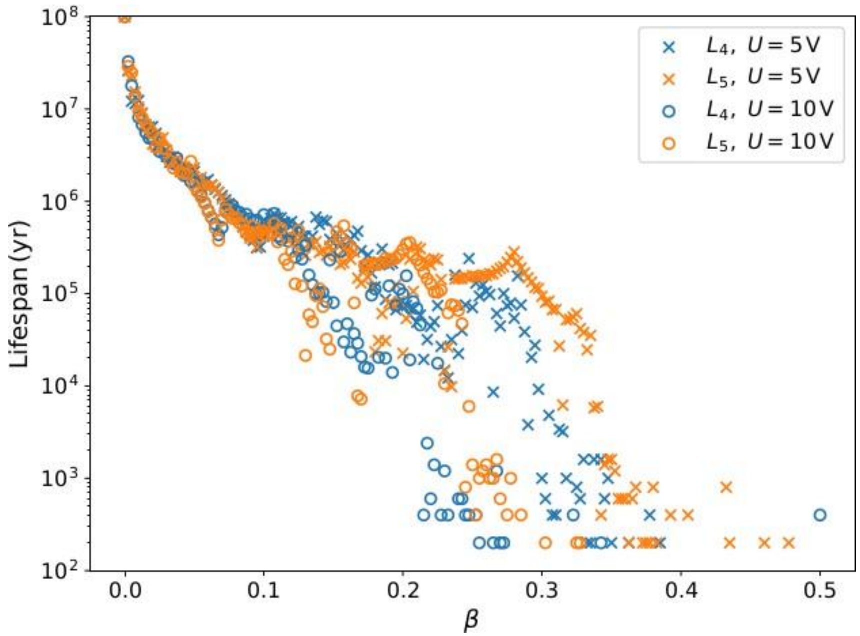

- Dependence on size (inverse to parameter beta) and charge-to-mass ratio (proportional to parameter gamma).

- Capture times also depend on mass of co-orbital planet (Jupiter vs. Venus) and distance from the sun.

Specific role of charge III/III

- Particle motion determined by interplay of radiation due to the sun and heliospheric magnetic field.
- Larger size-to-mass and charge-to-mass ratios experience stronger non-gravitational perturbations
- Physical parameters (radius, density, etc..) of particles determine orbital lifetimes close to resonance.

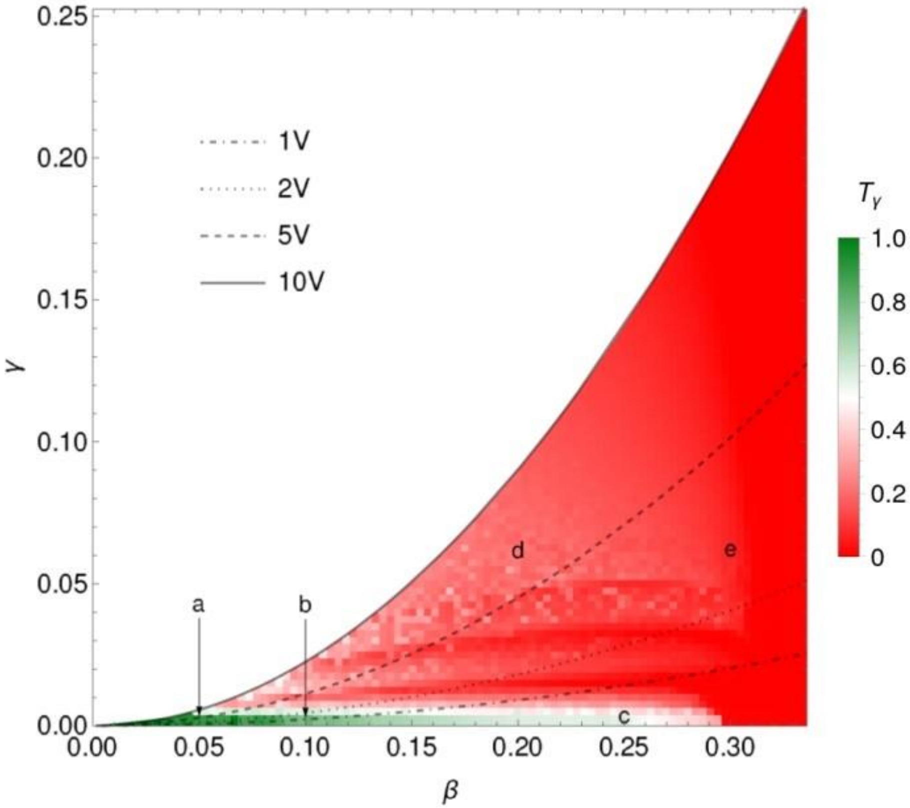

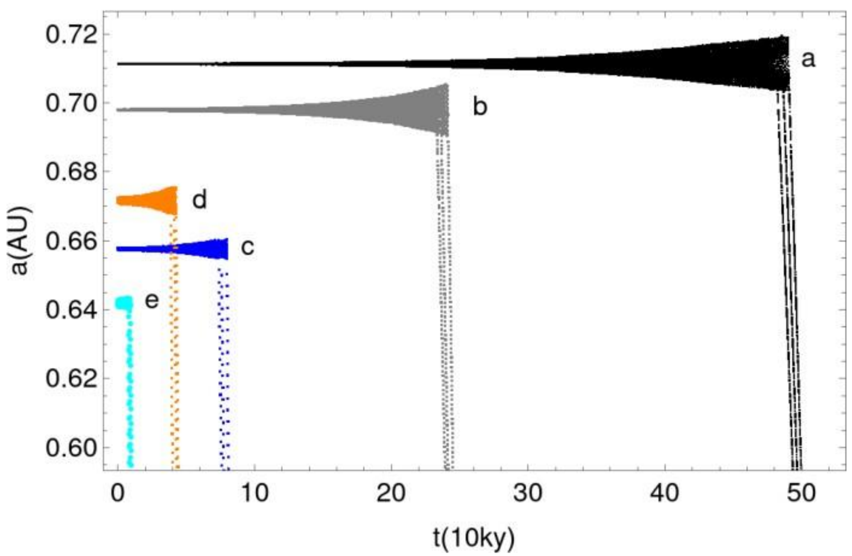

Zhou et al. 2021

Latitudinal variations

Lhotka & Gales 2019

Numerical vs. analytical models

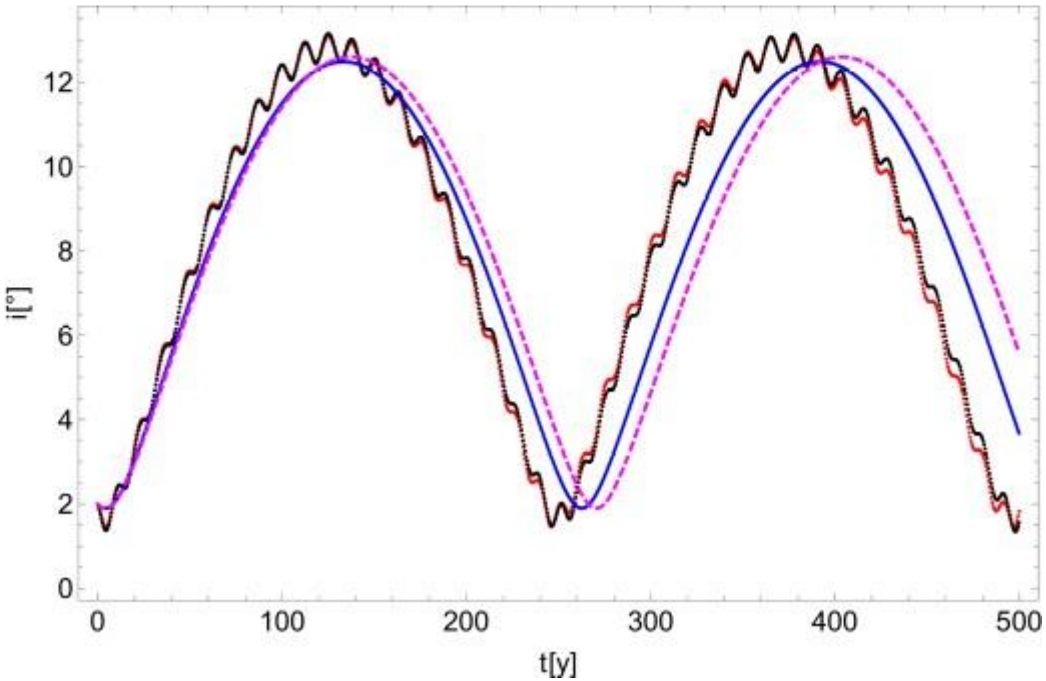

inclination

sun's rotation period

$$\Omega(t) = \left(\cos(i)\frac{\Omega_s}{n} - 1\right)\Gamma t + \Omega(0)$$

background

$$\Gamma = \alpha \frac{q}{m}\frac{B_0}{2}\left(\frac{r_0}{a}\right)^2$$

charge-to-mass ratio

semi-major axis

Reduced dynamical model :

$$m\ddot{\mathbf{r}} = \mathbf{F}_{Kep} + \mathbf{F}_L$$

Kepler

Lorentz force

cyclic variations of the orbital plane

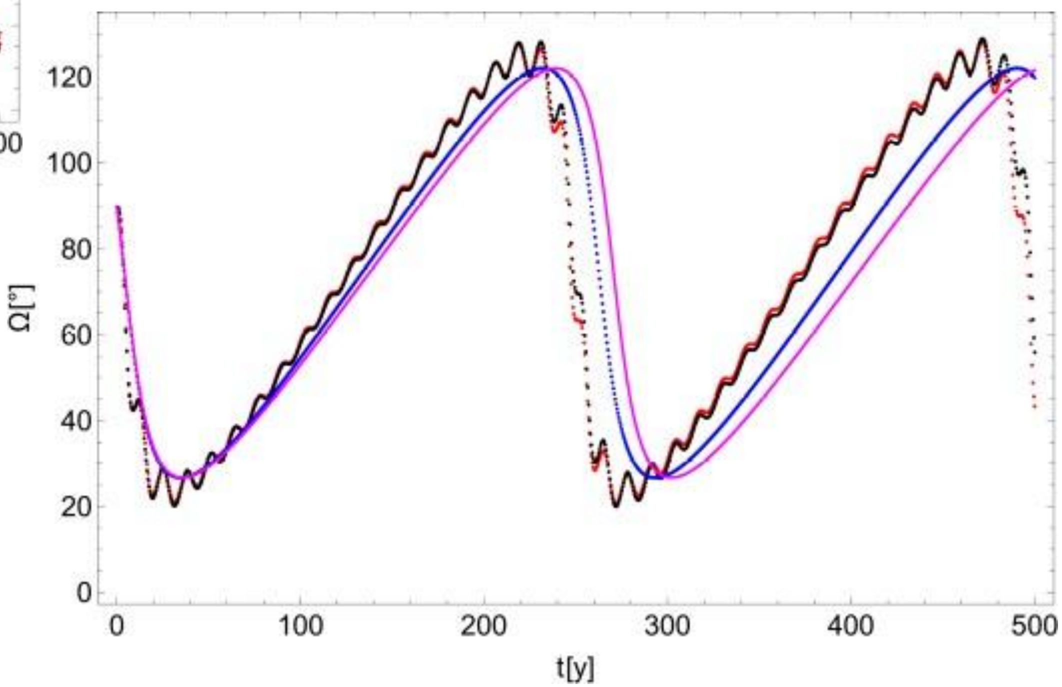

Spatial distribution of dust

Numerical vs. analytical models

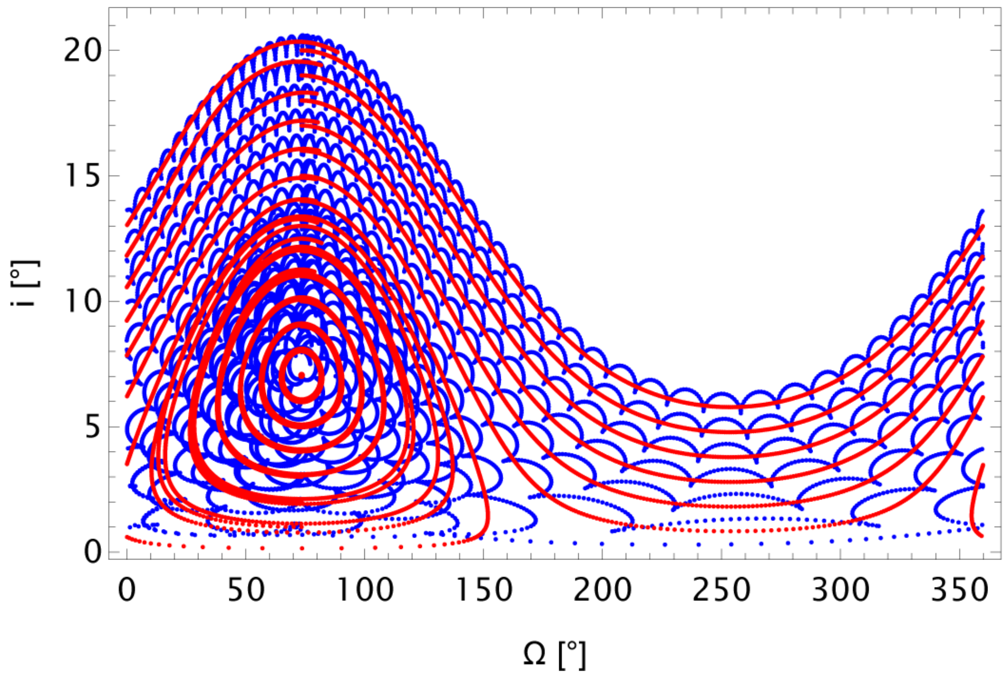

Reiter, Lhotka 2022

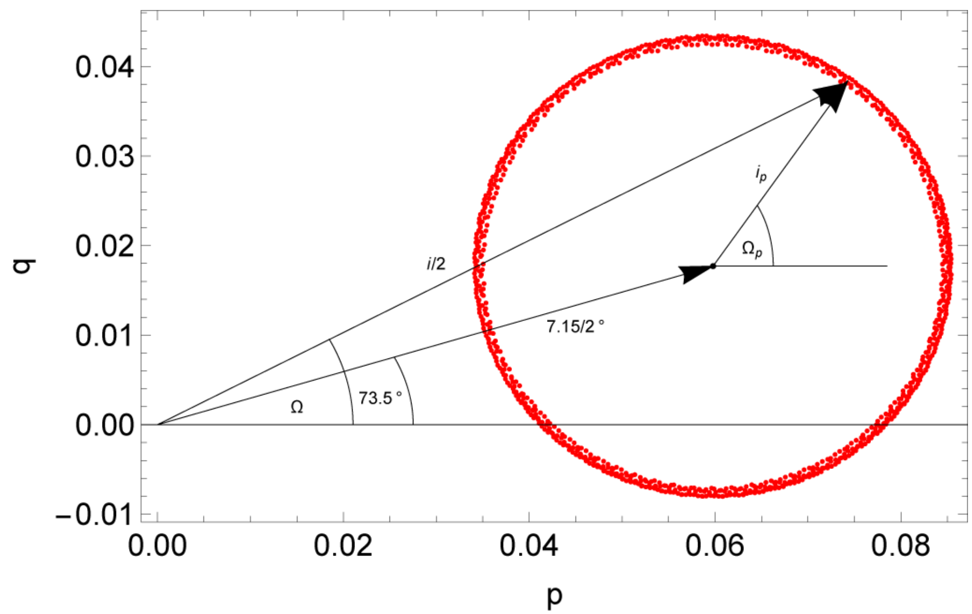

background

$$\Gamma = \alpha \frac{q}{m} \frac{B_0}{2} \left(\frac{r_0}{a} \right)^2$$

charge-to-mass ratio

semi-major axis

Ascending node period and variations in inclinations are given by deviation between angular momentum and magnetic axis

Spatial distribution of charged dust

Reiter, Lhotka 2022

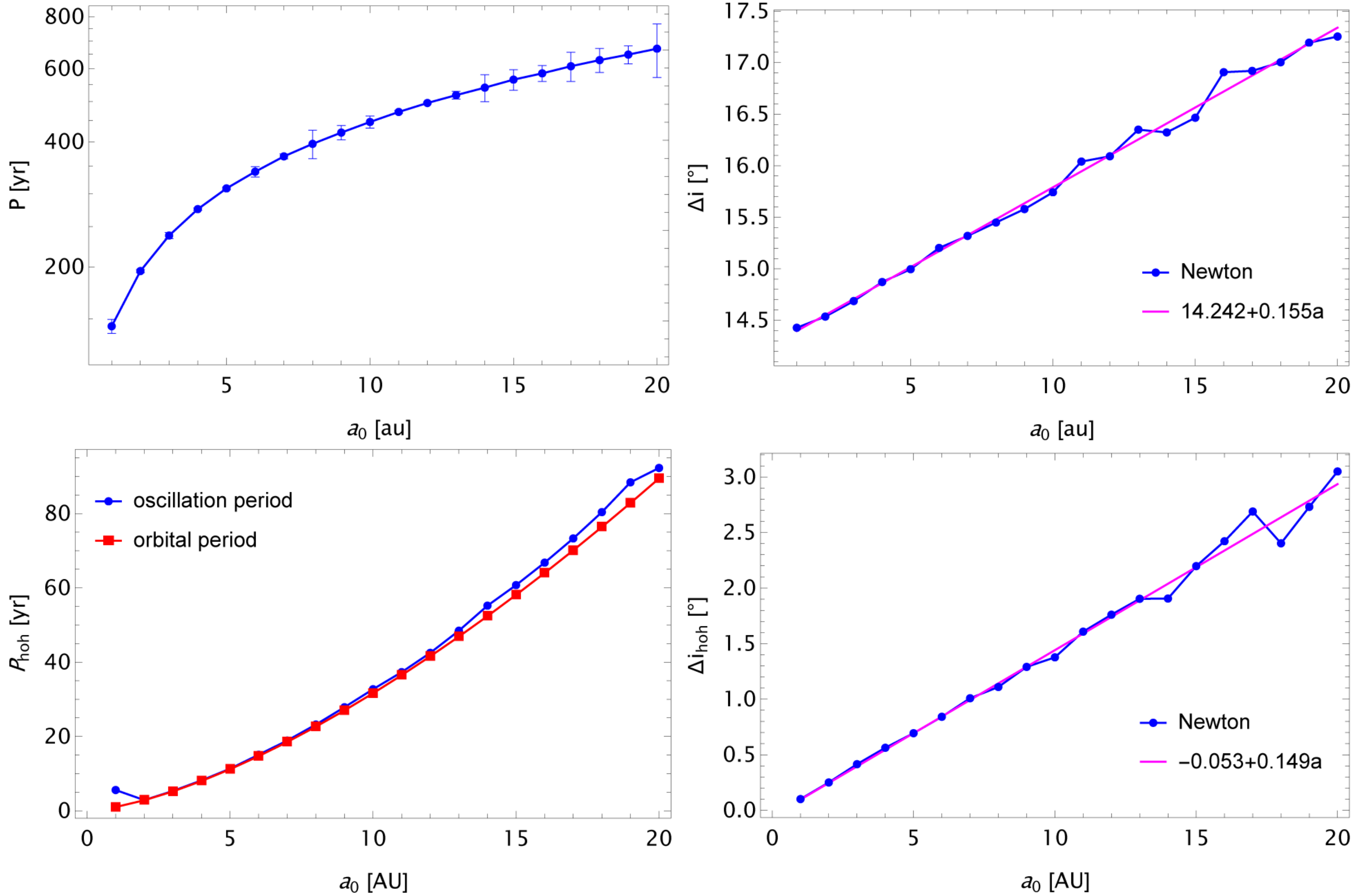

Latitudinal excursions depend on solar distance, debris size, and space weather effects

IMF partitions dust in planetary systems

Maximum excursions in latitude (amplitudes) and periods depend on size of the dust particles.
Fragments of break-up events are getting partitioned by the IMF into groups of similar size and densities.

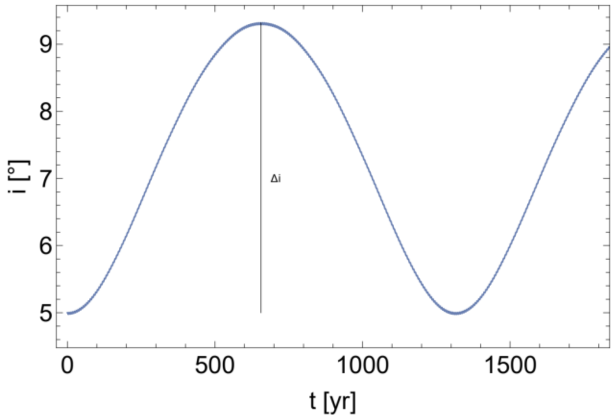

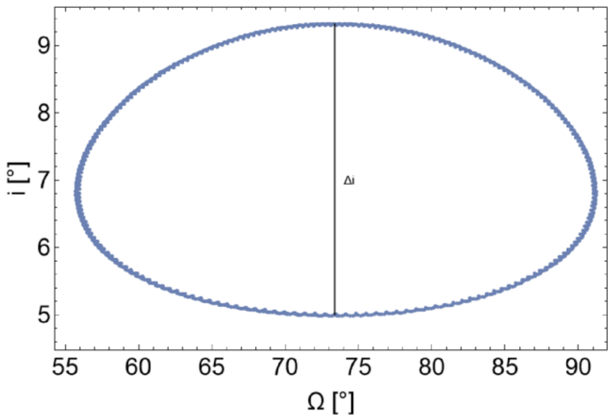

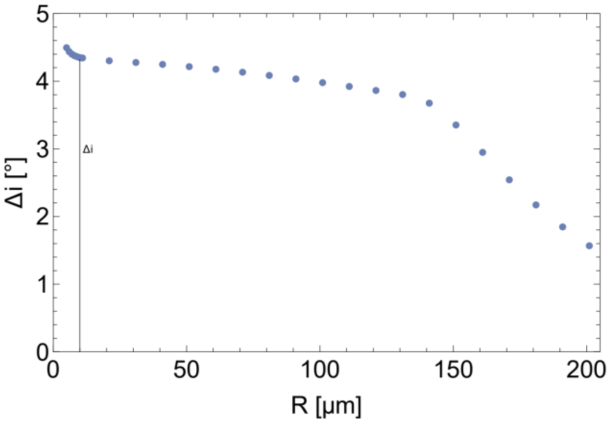

Reiter, Lhotka 2023

‘Saturation curve’ of breakup events

Reiter, Lhotka 2023

Lorentz dominated

saturated

Maximum excursion ... dust particles.
Fragments of break- ... similar size and densities.

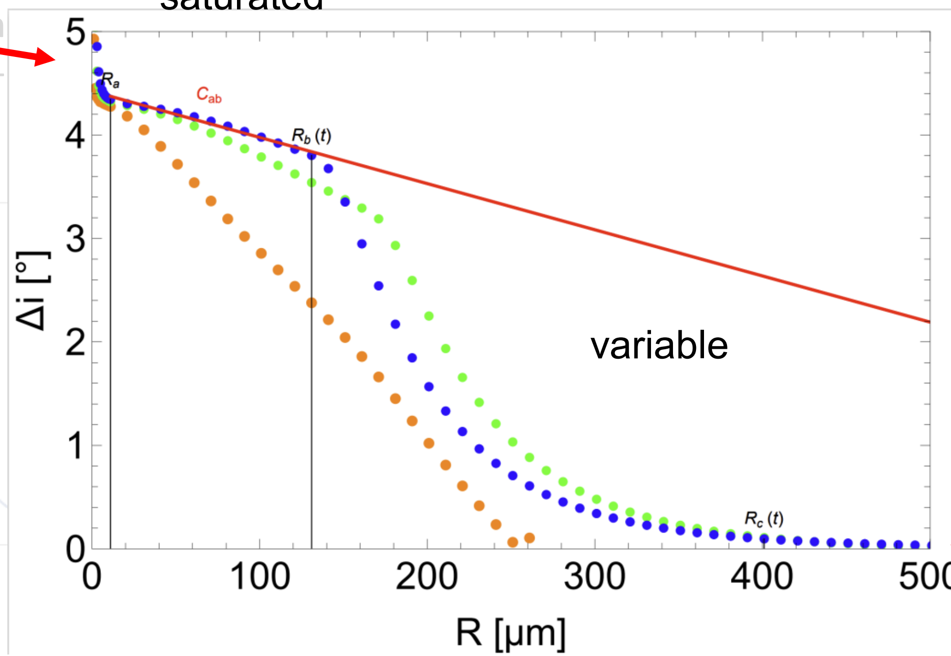

Shape depends on:

- solar activity
- solar distance

- orbital life time
- nearby planets

gravity dominated

Dust bands formed by the IMF

Dust bands in the zodiacal light formed at different ecliptic latitudes from cometary dust, fragments of break-up events or collisions of asteroids and meteoroids in space.

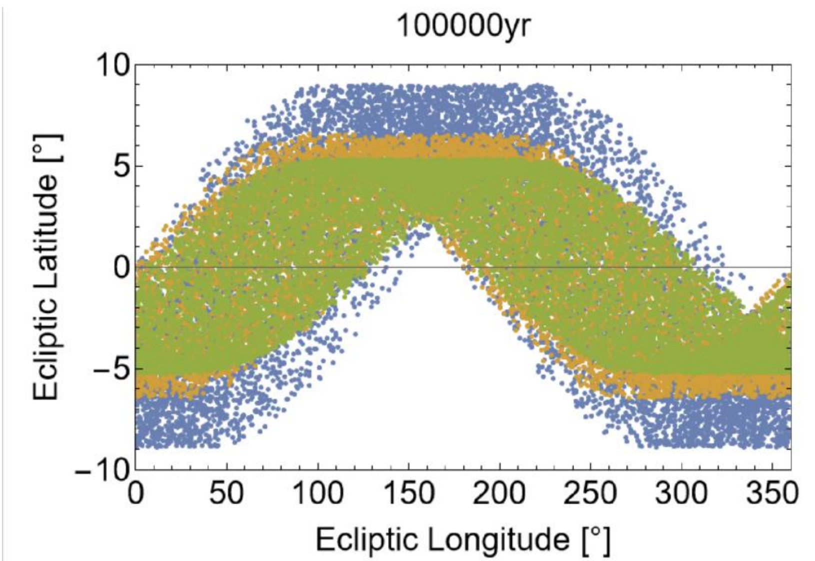

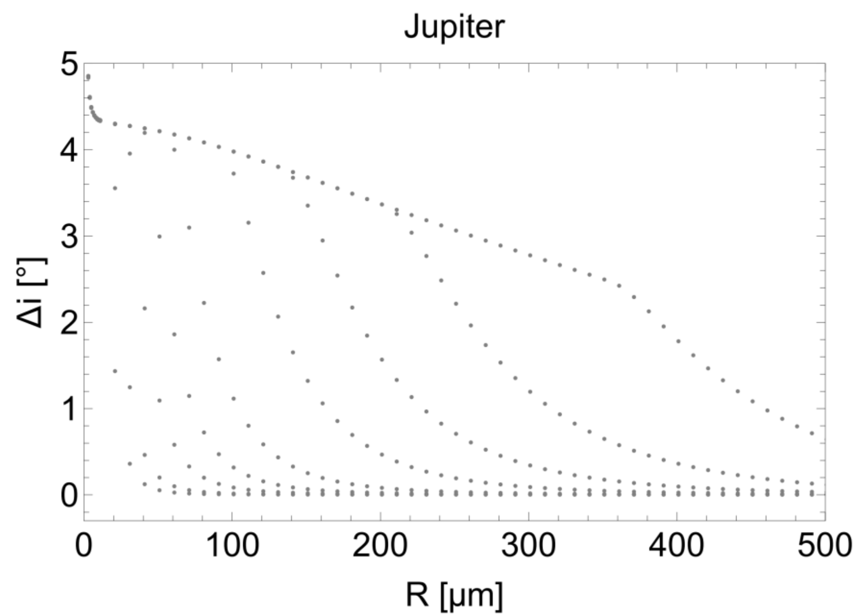

Reiter, Lhotka 2023

Dust charging model I/II

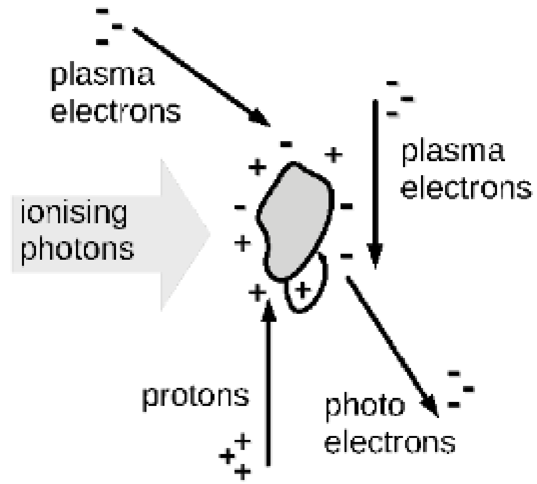

Set-up of mathematical model for charging processes

Current balance equation:

charge

currents

$$\frac{dq}{dt} = \sum_{k=1}^{N} I_k$$

plasma parameters

Electron current:

$$I_e = -\sqrt{8\pi} r_d^2 q_e n_e v_{T_e} \exp\left(\frac{q_e \phi_d}{k_B T_e}\right)$$

dust parameter

Ion current (protons or ions):

$$I_i = \sqrt{8\pi} r_d^2 q_e n_i v_{T_i} \left(1 - \frac{q_e \phi_d}{k_B T_i}\right)$$

surface potential

Equation for charge number:

$$\frac{dZ_d}{dt} = -\frac{I_e + I_i}{q_e}$$

Lhotka et al. 2020

Dust charging model II/II

Normalized charge number

$$\frac{dz_n}{dt} = -\alpha_n \left(1 + \frac{T_e}{T_i} z_n - \frac{v_{T_e}}{v_{T_i}} e^{-z_n}\right)$$

Equation in normalized units

plasma temperatures

mean particle velocities

$$1 + \frac{T_e}{T_i} z_0 - \frac{v_{T_e}}{v_{T_i}} e^{-z_0} = 0$$

Equilibrium charge condition

$$z_n = z_0 + z_1$$

$$\frac{dz_1}{dt} = -\alpha_n \left(\frac{T_e}{T_i} + \frac{v_{T_e}}{v_{T_i}} e^{-z_0}\right) z_1$$

Linearized equation of motion

$$t_c \propto \frac{1}{\alpha_n \left(\frac{T_e}{T_i} + \frac{v_{T_e}}{v_{T_i}} e^{-z_0}\right)}$$

$$z_1(t) \propto e^{-t/t_c}$$

Charging time scale

Parameter that collects all physics:

$$\alpha_n = \frac{\sqrt{8\pi} r_d n_0 q_e^2 v_{T_i}}{k_B \varepsilon_0 T_e}$$

Lhotka et al. 2020

Charging time scales

Kappa vs. Maxwellian plasma particle distribution functions:

$$t_c = \frac{1}{\alpha_{p,\kappa}\left[\left(\kappa - 1\right)\alpha' + e^{-z_0}\alpha_0\right]} \quad \text{vs.} \quad t_c \propto \frac{1}{\alpha_p\left(\frac{T_p}{T_e} + e^{-z_0}\right)}$$

with

$$\alpha_{p,\kappa} = \frac{2\sqrt{\pi}q_e^2 r_d n_0 \theta_e}{k_B T_p \varepsilon_0} \qquad \alpha' = \frac{T_p}{T_e}\frac{2}{(2\kappa - 3)} \qquad \alpha_p = \frac{\sqrt{8\pi} r_d n_e q_e^2 v_{T_e}}{k_B \varepsilon_0 T_p}$$

Electron – ion plasma without photoelectric effect:

$$t_c \propto \frac{1}{\alpha_{n,k}\frac{(\kappa-1)}{\kappa}\left[\frac{T_e}{T_i} + \frac{v_{T_e}}{v_{T_i}}\left(\frac{z_0+\kappa}{\kappa}\right)^{-\kappa}\right]} \quad \text{vs.} \quad t_c \propto \frac{1}{\alpha_n\left(\frac{T_e}{T_i} + \frac{v_{T_e}}{v_{T_i}}e^{-z_0}\right)}$$

In the limit (kappa →infty) the time-scales (and equilibria) coincide

Lhotka et al. 2020

Charging processes I/II

charge currents

Current balance equation : $dq/dt = \sum_k I_k$

Main charging processes in the solar system:

- Impacts of electrons and ions which transfer their charge to the grain
- Photo electron emission induced by solar photons
- Secondary electron currents, etc.

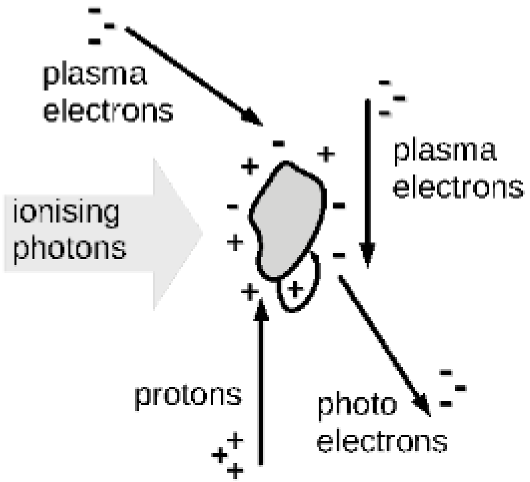

Equilibrium charge when sum of currents vanish:

$$\frac{\mathrm{d}q_D}{\mathrm{d}t} = I_e + I_i + I_\nu + I_{sec} = 0$$

electrons / ions

Photo electrons

Secondary emissions

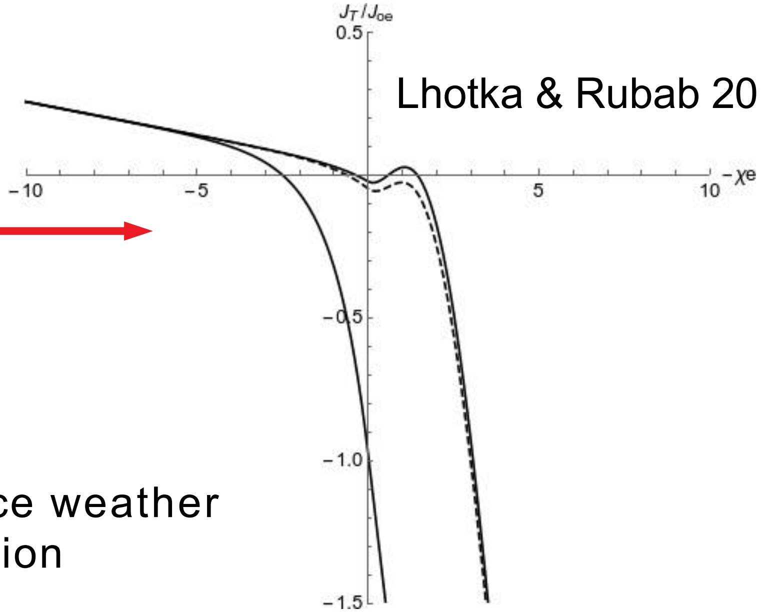

Lhotka & Rubab 2019

Constant charge depends on distance from the sun, space weather conditions as well as particle size and chemical composition

Charging processes II/II

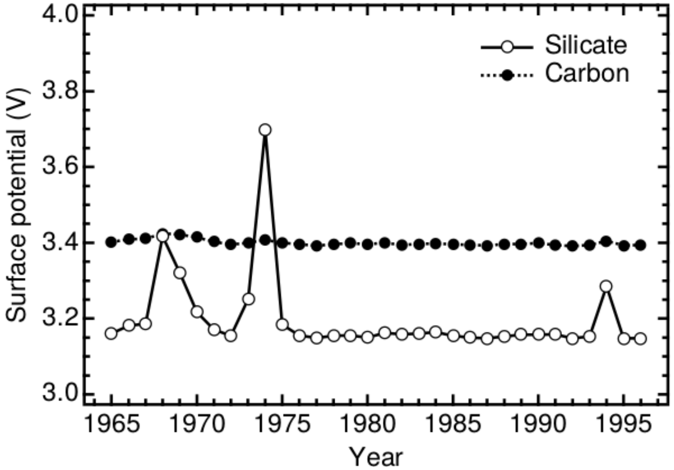

Temporal variation due to different solar wind conditions of the surface potential of a grain having mass of 3×10^{-16}kg located at 1AU.

Surface potential of interstellar dust grains vs. grain size at different heliocentric distances from the sun.

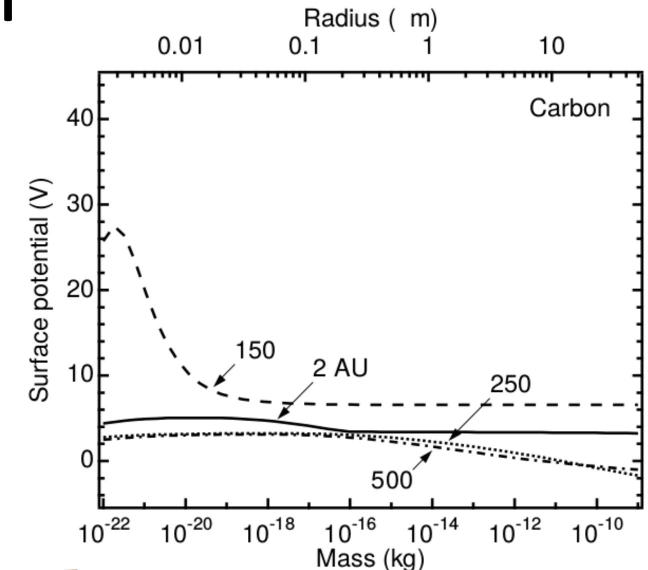

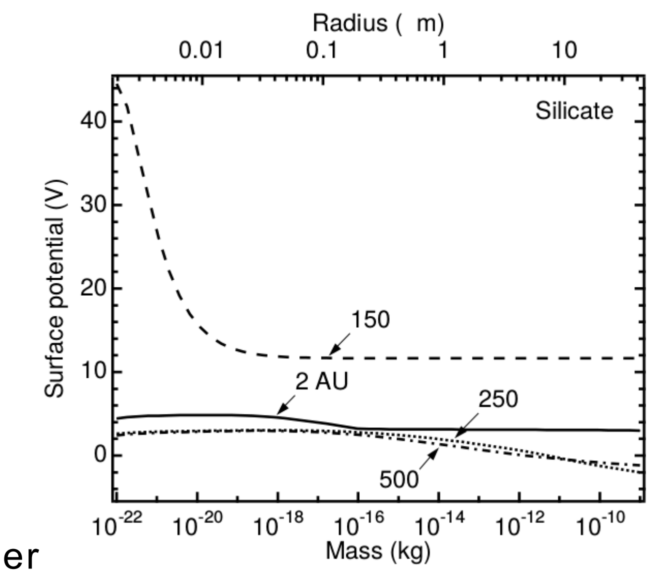

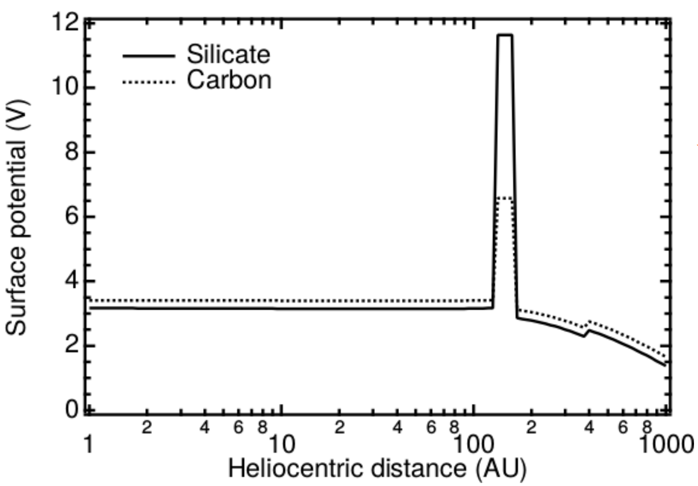

Surface potential of interstellar dust grains having mass 3×10^{-16}kg vs. heliocentric distances ranging from 1 to 1000 AU.

Constant charge depends on distance from the sun, space wea ther conditions as well as particle size and chemical composition

Mann

Maxwellian distribution

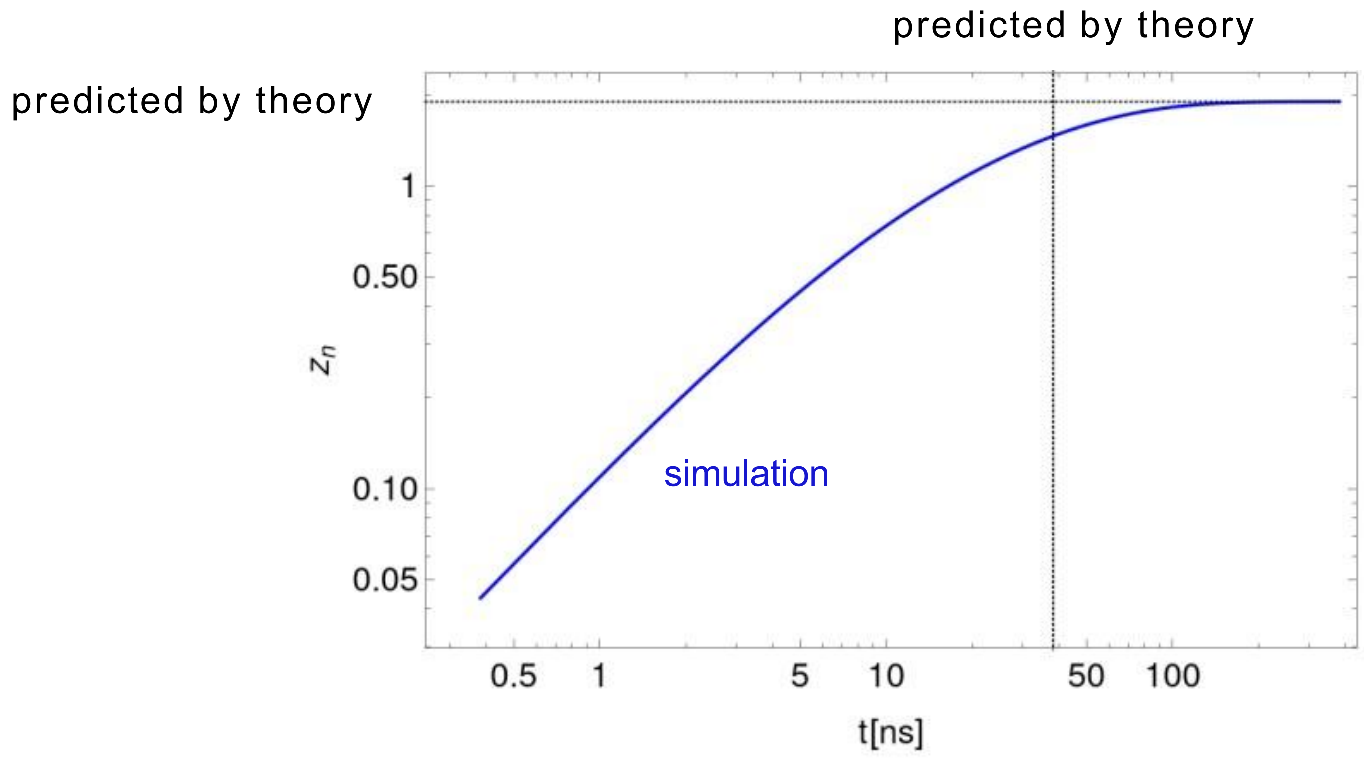

Corresponds to about -5V in physical units

Comparison with measurements will follow later!

Fig. 1: Charging history for the case 1a-r with $r_d = 1\mu m$, $T_e/T_i = 10$, $n_0 = 5 \cdot 10^9 cm^{-3}$, and $m_i = m_p$ (the proton mass).

Lhotka et al. 2020

Further reading

Reiter & Lhotka 2023 https://doi.org/10.1093/mnras/stad1848

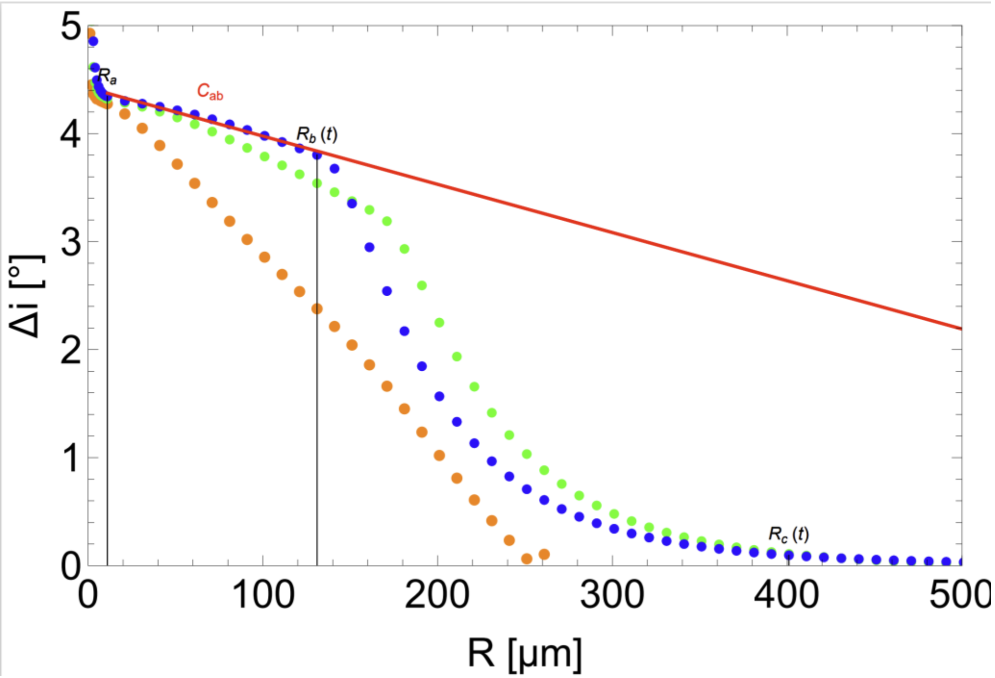

Beauge & Ferraz-Mello 1994
https://doi.org/10.1006/icar.1994.1119

Klacka et al. 2014
https://doi.org/10.1016/j.icarus.2012.06.044

Lhotka & Celletti 2015
https://doi.org/10.1016/j.icarus.2014.11.039

Lhotka et al. 2016
https://doi.org/10.3847/0004-637X/828/1/10

Lhotka & Narita 2019
https://doi.org/10.5194/angeo-37-299-2019

Lhotka & Gales 2019
https://doi.org/10.1007/s10569-019-9928-y

Lhotka & Rubab 2019
https://doi.org/10.1063/5.0018170

Lhotka & Zhou 2021
https://doi.org/10.1016/j.cnsns.2021.106024

Pokorny & Kuchner 2019
https://doi.org/10.3847/2041-8213/ab0827

Reiter & Lhotka 2022
https://doi.org/10.1051/0004-6361/202243693

Zhou & Lhotka 2021
https://doi.org/10.1051/0004-6361/202039617

Further reading

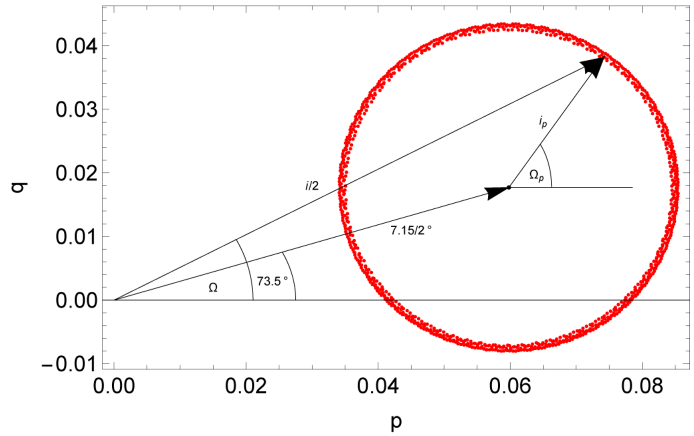

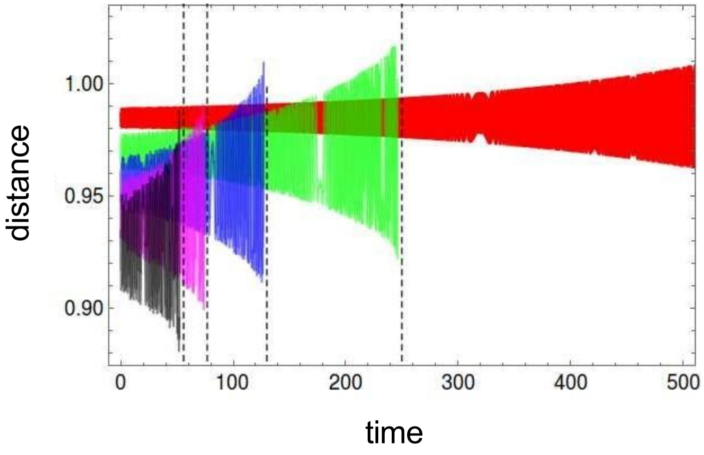

Beauge & Ferraz-Mello 1994
https://doi.org/10.1006/icar.1994.1119

Klacka et al. 2014
https://doi.org/10.1016/j.icarus.2012.06.044

Lhotka & Celletti 2015
https://doi.org/10.1016/j.icarus.2014.11.039

Lhotka et al. 2016
https://doi.org/10.3847/0004-637X/828/1/10

Lhotka & Narita 2019
https://doi.org/10.5194/angeo-37-299-2019

Lhotka & Gales 2019
https://doi.org/10.1007/s10569-019-9928-y

Lhotka & Rubab 2019
https://doi.org/10.1063/5.0018170

Lhotka & Zhou 2021
https://doi.org/10.1016/j.cnsns.2021.106024

Pokorny & Kuchner 2019
https://doi.org/10.3847/2041-8213/ab0827

Reiter & Lhotka 2022
https://doi.org/10.1051/0004-6361/202243693

Zhou & Lhotka 2021
https://doi.org/10.1051/0004-6361/202039617

Further reading

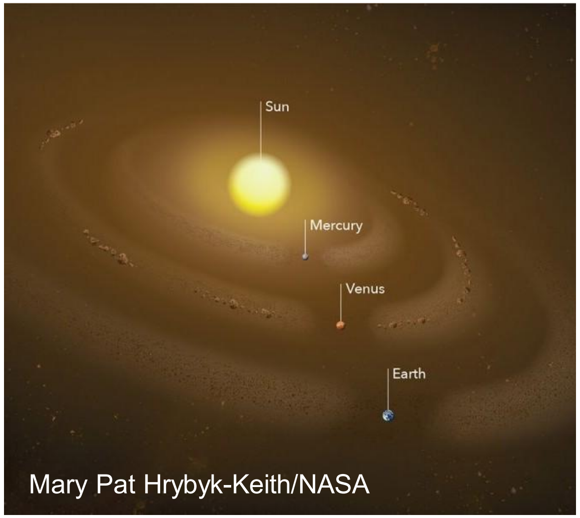

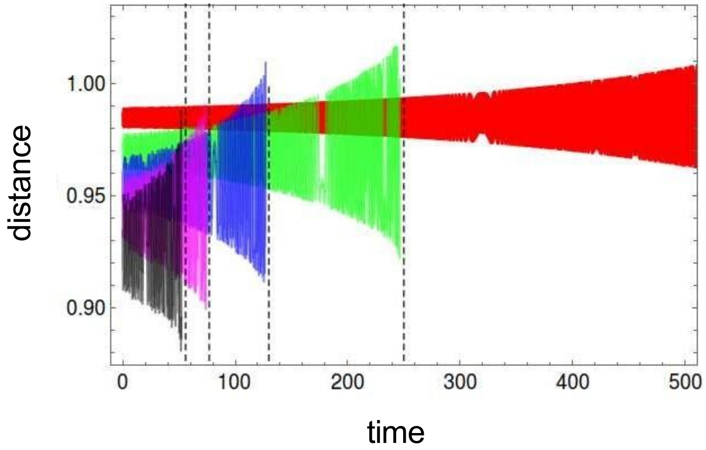

Beauge & Ferraz-Mello 1994
https://doi.org/10.1006/icar.1994.1119

Fedele et al. 2017
https://doi.org/10.1051/0004-6361/201629860

Klacka et al. 2014
https://doi.org/10.1016/j.icarus.2012.06.044

Lhotka & Celletti 2015
https://doi.org/10.1016/j.icarus.2014.11.039

Lhotka et al. 2016
https://doi.org/10.3847/0004-637X/828/1/10

Lhotka & Narita 2019
https://doi.org/10.5194/angeo-37-299-2019

Lhotka & Gales 2019
https://doi.org/10.1007/s10569-019-9928-y

Lhotka & Rubab 2019
https://doi.org/10.1063/5.0018170

Lhotka & Zhou 2021
Accepted (arxiv: https://doi.org/10.1016/j.cnsns.2021.106024)

Pokorny & Kuchner 2019
https://doi.org/10.3847/2041-8213/ab0827

Zhou & Lhotka 2021
https://doi.org/10.1051/0004-6361/202039617

In plane vre

Classical (time dependent) Parker spiral model :

$$B_R = B_0 \left(\frac{r_0}{r}\right)^2 b_R(t) \qquad b_R\,(t) = \cos\left(2\pi t/T + \varphi_0\right)$$

$$B_T = B_0 \left(\frac{r_0}{r}\right) b_T(t) \qquad b_T\,(t) = \cos\left(\vartheta\right) \cos\left(2\pi t/T + \varphi_0\right)$$

Importance of the normal component :

$$B_N = B_0 \left(\frac{r_0}{r}\right)^\kappa b_N(t) \qquad b_N(t) = 1 + \cos\left(2\pi t/T\right)$$

Study in distance for different κ (1=black, 2=red, 3=blue) :

- Mimics solar cycle with period T
- Radial component falls with $1/r^2$
- Tangential component falls with $1/r$
- Normal component falls with $1/r^\kappa$
- Non-zero mean of normal component

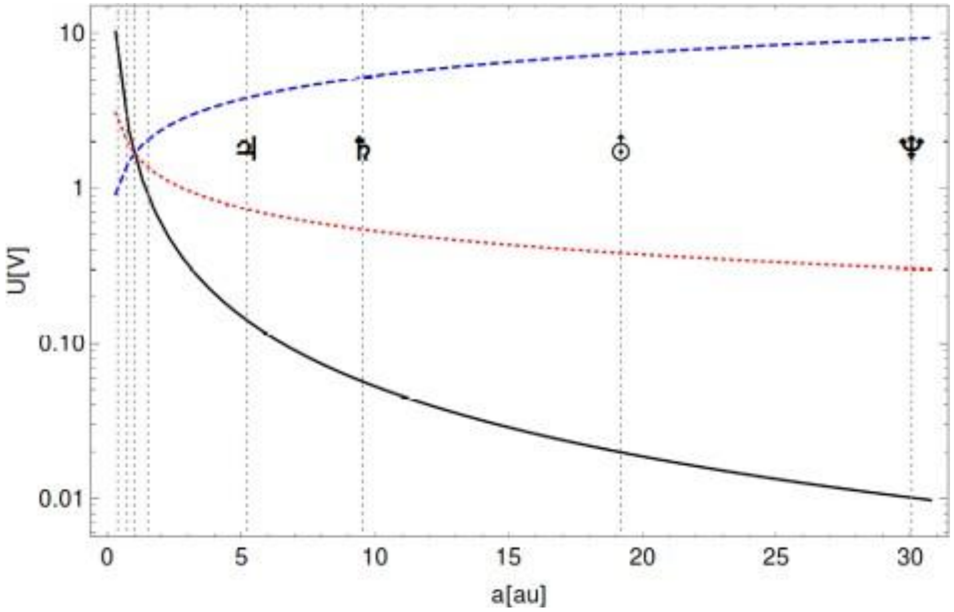

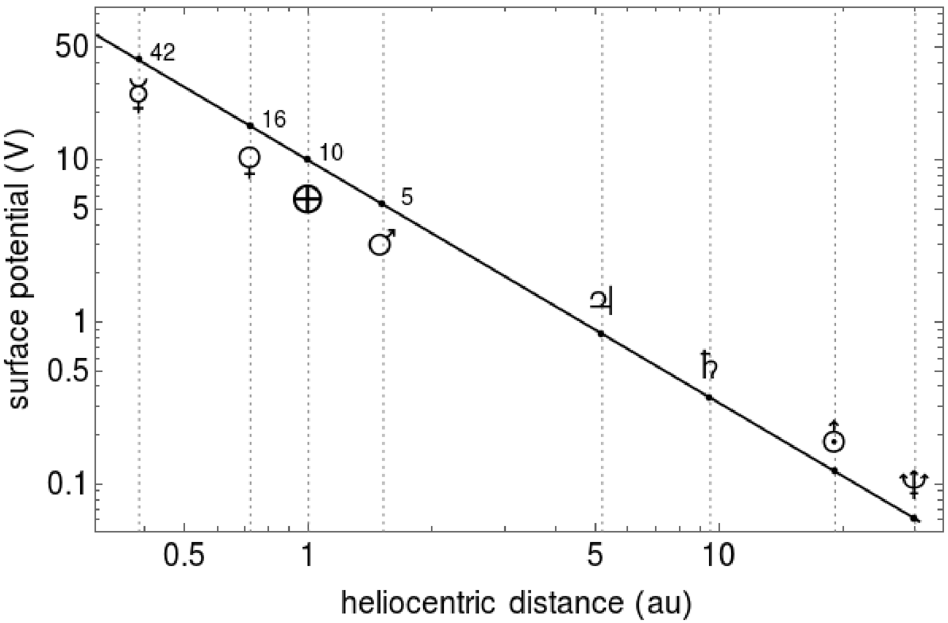

Out-of-plane motion

Reiter, Lhotka 2022

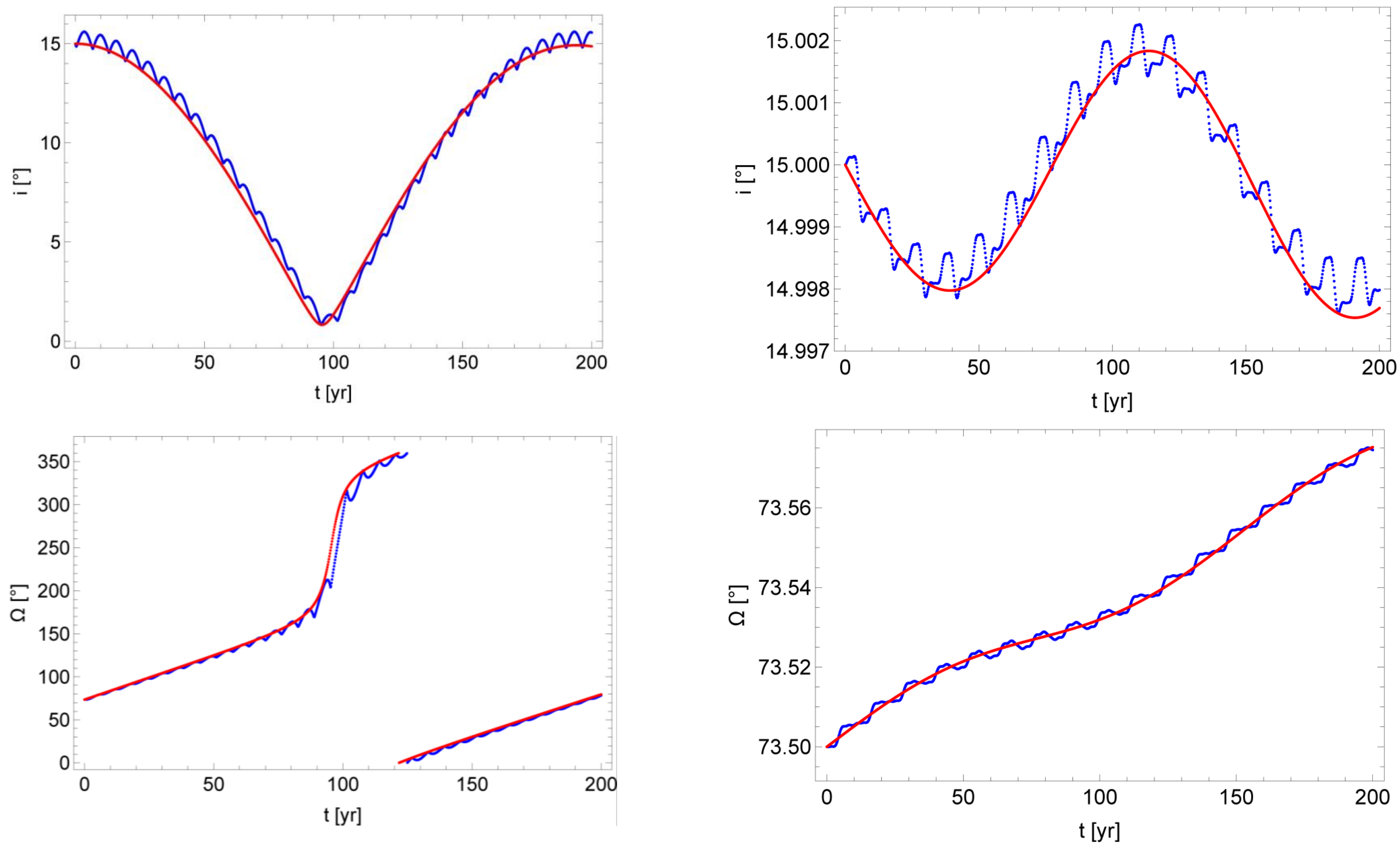

Lorentz force due to interplanetary magnetic field brings dust to high ecliptic latitudes